Journal of CO2 Utilization 114 (2026) 103619

Contents lists available at ScienceDirect

Journal of CO2 Utilization

journal homepage: www.elsevier.com/locate/jcou

Ultrafast kilowatt-range microwave pulsing for enhanced CO_2 conversion in atmospheric-pressure plasmas

S. Soldatov [a,*], L. Silberer [a], C.K. Kiefer [c,1,2], G. Link [a], A. Navarrete [b], J. Jelonnek [a]

[a] Institute for Pulsed Power and Microwave Technology (IHM), Karlsruhe Institute of Technology (KIT), Kaiserstraße 12, Karlsruhe 76131, Germany
[b] Institute for Micro Process Engineering (IMVT), Karlsruhe Institute of Technology (KIT), Hermann-von-Helmholtz-Platz 1, Eggenstein-Leopoldshafen, 76344, Germany
[c] Max-Planck-Institut für Plasmaphysik, Boltzmannstraße 2, Garching, 85748, Germany

ARTICLE INFO

Keywords:
CO2 conversion
Microwave plasma
Atmospheric-pressure plasma
Pulsed microwave
Power modulation

ABSTRACT

While ultrafast microwave power pulsation has previously been shown to enhance CO_2 conversion in atmospheric-pressure plasmas at moderate power levels, its applicability to kilowatt-range reactors remains unclear. The present study investigates the scalability of this approach by comparing CO_2 conversion and energy efficiency in two high-power reactor configurations – a Surfaguide-based system (KIT) and a cavity-based plasma torch at IPP – with corresponding results obtained using a compact coaxial plasma torch. The two kilowatt-scale systems operate at peak powers of approximately 4 kW but differ substantially in afterglow treatment: the cavity-based torch at IPP employs a water-cooled nozzle, whereas the Surfaguide-based reactor features an extended quartz tube. Stable pulsed operation was limited to inter-pulse times of approximately 10 μs and 12 μs in the cavity-based torch at IPP and the Surfaguide-based reactor, respectively. Unlike the coaxial torch, no pronounced plasma reignition regime was observed in either kilowatt-scale reactor, while substantially weaker gas-temperature modulation was measured in the Surfaguide-based reactor. In the latter, the period-averaged gas temperature exceeded that under continuous-wave operation, and relative enhancements of up to 36% in CO_2 conversion and 30% in energy efficiency were obtained. No corresponding improvement was observed in the nozzle-equipped cavity-based torch at IPP, suggesting an important role of reactor-specific post-plasma treatment. Time-resolved reflected microwave power further provided qualitative information on the evolution of the plasma electromagnetic load during power modulation.

1. Introduction

The capture of carbon dioxide (CO_2) from the atmosphere or from industrial exhausts with its consecutive conversion into value-added chemicals is believed to reduce greenhouse gas emissions on our planet and mitigate global warming. Particularly, the electro-chemical conversion of CO_2 when it is driven by electricity from renewable energy sources, like wind and solar, draws special attention. The use of renewable electricity, which is intermittent by nature, for production of synthetic hydrocarbons from captured CO_2 allows the storage of surplus electrical energy from renewables when the supply exceeds the demand. Liquid fuels synthesized with captured CO_2 and renewable electricity can replace the fossil-based kerosene [1], gasoline and diesel and enable the closing of the carbon cycle in the transport sector. The two main electro-chemical approaches for CO_2 conversion are based on electrolysis and plasma. Plasma-assisted CO_2 conversion features a quick start and stop of process that matches fluctuating renewable electricity very well [2], high energy density, and no use of rare-earth materials. Among different types of plasma-based reactors, microwave (MW) plasma reactors have shown the most promising results so far with energy efficiency of up to 90% [3–5], though at vacuum conditions. The operation of microwave plasma reactors at atmospheric pressure instead of vacuum is favorable for the industrial applications, because it reduces the energy consumption and capital expenditures compared to vacuum systems. However, the CO_2 conversion decreases with increasing pressure. For the CO_2 splitting reaction which reads as

* Corresponding author.
E-mail address: sergey.soldatov@kit.edu (S. Soldatov).
[1] Current affiliation: Research group PLASMANT and Center of Excellence PLASMA, Department of Chemistry, University of Antwerp, Universiteitsplein 1, Antwerp, 2610, Belgium
[2] Current affiliation: Electrification Institute, University of Antwerp, Olieweg 97, 2020 Antwerp, Belgium

https://doi.org/10.1016/j.jcou.2026.103619
Received 1 April 2026; Received in revised form 7 October 2026; Accepted 4 November 2026
Available online 17 November 2026
2212-9820/© 2026 The Authors. Published by Elsevier Ltd. This is an open access article under the CC BY license (http://creativecommons.org/licenses/by/4.0/).
Open access funding enabled and organized by Projekt DEAL.

$$CO_2 \rightarrow CO + \frac{1}{2}O_2 + 2.93 \quad eV \tag{R1}$$

the deterioration both conversion and energy efficiency in microwave plasma discharge at pressures above 0.3 bar is mostly linked to the CO recombination reactions [6]:

$$CO + O + M \rightarrow CO_2 + M \tag{R2}$$

$$CO + O_2 \rightarrow CO_2 + O \tag{R3}$$

where M stands for a collision partner. Berthelot et al. has shown that along with increasing pressure and temperature the rates of reactions R2 and R3 increase and CO_2 conversion degrades. For microwave reactors operating at near atmospheric pressure the extremely high gas temperatures (6000 –7000 K) [7–10] are unavoidable while CO_2 plasma at $p > 0.2$–0.3 bar experiences the transition from diffuse to contracted regime, and its temperature rises steeply [7]. This phenomenon of plasma contraction described in [11] is characterized by formation of a hot plasma filament whose cross-section size can be significantly smaller than diameter of reactor tube [7,12]. At such plasma conditions, the rapid quenching is crucial to avoid the deterioration in conversion and efficiency [6,13]. Particularly in microwave plasmas, experiments employing active gas quenching via water-cooled metallic structures in the afterglow, such as a “gas shower” [14] and nozzle [15–17] have been reported, demonstrating a significant increase in reactor performance compared with setups without quenching.

Alternatively, to increase conversion and process efficiency at near-atmospheric pressures, the microwave (MW) power sustaining the plasma can be delivered in short pulses rather than continuously. Microwave pulsation has been used in different reactor configurations for investigation of both plasma dynamics [18–24] and chemical conversion [9,25–29]. Because of instant microwave-to-electrons energy coupling, the electron density, n_e, and temperature, T_e, are found to respond promptly to microwave power modulation [20,25,30]. The response in T_e was found to be much faster than in n_e and, if the inter-pulse time was long enough, the overshoot in electron temperature in the beginning of pulse was documented [20,30], Such T_e and n_e dynamics were also confirmed in global plasma model with pulsed energy [31] and multi-physics modelling for hydrogen plasma and pulsed microwave energy in [22]. Additionally, in experiments with H_2 plasmas (Rousseau et al., 1994 [18]) and in global model of Lieberman and Ashida for argon and chlorine plasmas [31] a higher mean electron density was reported in pulsed discharge as compared with continuous discharge. Moreover, the modulation of vibrational and gas temperatures in pulsed plasma experiments [21,22,25] and their relation to the energy efficiency supported with plasma modelling [32–34] were reported.

Vermeiren and Bogaerts in 0D model demonstrated that vibrationally driven dissociation in CO_2 plasma can be optimized by power pulsing through appropriate adjustment of the pulse duration and inter-pulse time at a pressure of 0.1 bar, a reduced electric field of 50–150 Td, and a specific energy input (*SEI*) of approximately 1 eV molecule^{-1} [33]. In that work, optimal pulse and inter-pulse times were found to result from a trade-off between the time required to reach maximum over-population of high vibrational levels and the vibrational–translational (V–T) relaxation time, which decreases with increasing gas temperature. Experimentally, a similar optimum was identified for an atmospheric MW plasma in a coaxial plasma torch at $0.02 < SEI < 0.22$ eV molecule^{-1} [9]. In that study, microwave power pulsation more than doubled the CO_2 conversion and energy efficiency relative to the corresponding CW values at comparable *SEI*. In addition, clear evidence of non-equilibrium between the rotational (T_{rot}) and vibrational (T_{vib}) temperatures was observed, with a maximum ratio of $T_{vib} / T_{rot} \approx 2$. These findings motivated pulsation experiments in larger plasma reactors operating at kilowatt MW power and at *SEI* values from 1 to 5 eV molecule^{-1} , using two reactor configurations: (i) a Surfaguide-based [35] reactor installed at Karlsruhe Institute of Technology (KIT), and (ii) a modular plasma torch consisting of a cylindrical and coaxial resonator allowing plasma self-ignition installed at Max Planck Institute for Plasma Physics (IPP) [15,36,37] which is referred further in text as cavity-based plasma torch at IPP.

In the present paper, we perform a detailed comparison of experimental results obtained in the two abovementioned configurations and relate them to results from pulse-plasma coaxial torch experiments reported in [9,26]. We investigate how kilowatt-range MW power pulsations with durations ranging from several hundred nanoseconds to several microseconds influence CO_2 conversion and energy efficiency in atmospheric microwave-sustained plasmas. The rest of paper is organized as follows. The experimental setups and diagnostic methods used in the three abovementioned studies are described in Section 2. The results are compared and discussed in Section 3, and conclusions together with an outlook for future experiments are presented in Section 4.

2. Setups and experimental methods

This section describes three microwave-sustained CO_2 plasma setups, all employing solid-state microwave (SSM) generators capable of operating in continuous-wave (CW) and power-modulated modes with pulse and inter-pulse durations of ≥ 50 ns. In the coaxial torch experiment a 300 W (maximum rated power) SSM generator with pulse rise and fall times of ~30 ns was used [9], whereas the in the Surfaguide-based and IPP experiments we employed TruPlasma 5000–04/2450 SSM generator from TRUMPF Hüttinger GmbH with pulse edge times of ~15 ns and nominal power of 4 kW [38]. In both cases, the microwave power is adjustable in discrete steps over the ranges 20–300 W and 20–4000 W, respectively, and the operating frequency is tunable stepwise within 2.4–2.5 GHz. Frequency tuning is essential for reliable plasma ignition in the coaxial torch configuration.

2.1. Coaxial microwave torch experiment (KIT)

Details of the coaxial plasma torch experiment have been reported previously in [9]. In the present paper, this experiment is recalled only as a reference case, as it serves as a baseline for comparison with the two other reactor configurations investigated here. Accordingly, only the essential parameters are summarized below. The plasma reactor was an industrial coaxial plasma torch [39]; a photograph of a pure CO_2 plasma sustained at 220 W is shown in Fig. 1. Plasma ignition occurred spontaneously at a frequency tuned to 2.49 GHz and at MW power levels between 180 and 200 W. During operation, the torch was surrounded by a quartz tube with an inner diameter of 26 mm, which is significantly larger than the transverse dimension of the plasma plume (see Fig. 1).

In that studies, the volumetric concentration of products in effluent, the time resolved rotational and vibrational temperatures as well as time resolved absorbed power in the plasma were measured [9,26]. Additionally, time resolved fast imaging was utilized to follow a plasma evolution between two consecutive reignition events. Due to the converging geometry of the torch, the gas flow pattern is similar to a converging-diverging nozzle configuration [17], in which the gas flow first is accelerated in the nozzle neck and then decelerated in the diverging region. In the coaxial torch, the plasma is sustained at the top end of the torch and expands freely in the surrounding quartz tube, where it is quenched through convective mixing with cooler afterglow gas. The details of experiment and operation scenarios conducted in [9, 26] are summarized in Table 1.

2.2. Surfaguide-based reactor experiment (KIT)

The scheme of the Surfaguide-based reactor experiment is presented in Fig. 2. In this experiment, the Surfaguide-based [35] reactor was utilized to deliver MW power to a plasma confined in a quartz tube with

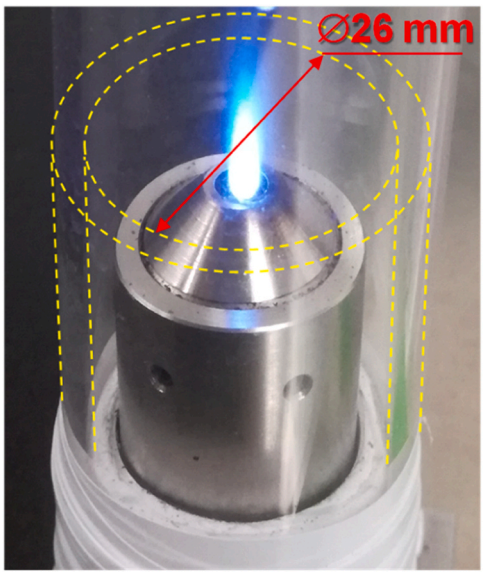


Fig. 1. Photo of the CO_2 plasma discharge sustained with CW microwave power of ~200 W and 12 slm inflow in a coaxial plasma torch. Thin dashed lines sketch the surrounding quartz tube.

an inner and outer diameters of 16 and 20 mm, respectively. As a part of the reactor, a chimney (a metallic tube surrounding the quartz tube with 110 mm in height) was installed to extend the coupling area of microwave to the plasma and to reduce the leakage of microwave to the surroundings. CO_2 Plasma ignition was achieved in a two-step process: first, an argon plasma was established, and subsequently, the argon was replaced by a CO_2 flow (99.998% purity) without extinguishing the discharge The initial argon plasma was ignited by applying a high-voltage pulse to the outer surface of the quartz tube, approximately 40 mm below the reactor. The ignition was successful using any argon flow rate within the range of 10–20 slm, combined with any CW microwave power between 0.9 and 1.5 kW. For high-voltage pulse generation, a standard automotive ignition-coil was utilized with the input voltage of 12 V. The output voltage was not explicitly measured but following the specifications for standard ignition-coils it is in the range 20 and 30 kV. Once a stable plasma was established, the microwave generator was either maintained in CW mode at the required power level or switched to pulsed mode. The transition from CW to pulsed operation was achieved at a relatively high duty cycle and short pulsation times (e.g., t_{on} = 5.0 μs, t_{off} = 5.0 μs) to initially stabilize the pulsed power discharge. Starting with this reference condition, the t_{on} and t_{off} times and the peak power were adjusted to achieve the target pulsed discharge scenarios.

The exhaust tube was open to atmosphere; consequently, within considered gas flow rates the pressure in the reactor was within a range of 1.01–1.05 atm due to the documented pressure drop in the heat exchanger installed in the exhaust line. The vortex configuration of the gas inflow was ensured by the geometry of the vortex injection system from Sairem. This system features two helically configured gas channels with an inner diameter of 2 mm. Such a vortex flow enabled efficient isolation of inner surface of reactor wall from the hot gas flowing near the axis of reactor tube. The amount of CO_2 gas supplied was controlled with a mass-flow controller. Next to the microwave generator output, the microwave circulator was installed to redirect and absorb the reflected wave and thus to minimize the secondary reflections inside waveguide system, that is an important condition for correct measurements of incident and reflected powers (Fig. 2). Between the circulator and reactor, a bidirectional microwave coupler (- 50 dB) served for decoupling the incident and reflected microwave for their subsequent detection.

Table 1
Summary of pulsed-operation scenarios in coaxial torch experiments at atmospheric pressure. More details can be found elsewhere in [9,26].

MW Power, W	CO_2 Flow, slm (at 25°C)	SEI, eV/molec	Typical Plasma Size, mm	Pulse Time, μs	Duty Cycle	Gas Supply	Afterglow & Quenching
80–250	12, 15, 18	0.02–0.22	h= 10–15 D= 2.5–3.5	0.1–50.0	0.1–0.99	Axial flow between inner and outer conductor	Free expansion to surrounding tube ⌀26 mm

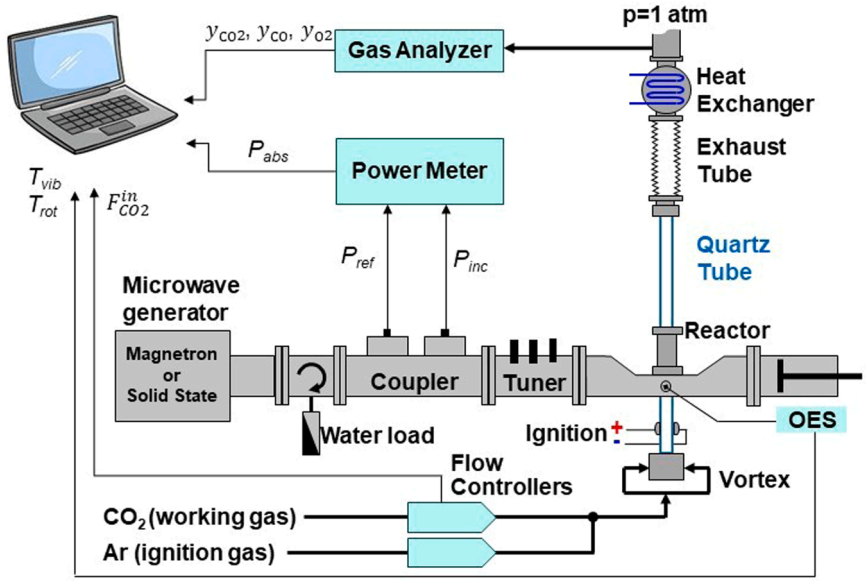


Fig. 2. Schematic illustration of the Surfaguide-based reactor experiment.

For later discussion on the efficiency of CO_2 conversion in the above system, it is important to describe the plasma afterglow in more detail. Plasma discharge was confined in relatively long quartz tube whose length above the reactor amounted to about 600 mm. To cool the reactor tube, the dry air flow between chimney inner surface and tube outer surface was supplied, whose flow was approximately 100 slm and temperature between 21 °C and 23 °C. For the rest of quartz tube no forced cooling was applied, and surface-to-surrounding radiation and convective heat exchange between tube surface and surrounding atmosphere (21–23 °C) took place. The end of the quartz tube was sealed to a glass-to-metal transition unit which was water-cooled. Right after this transition a gas-decoupling element was installed to branch a portion of the off-gas toward gas analyzer, where CO_2, CO and O_2 relative volume concentrations were recorded as described in Section 2.4.3. The gas probe position was located about 620 mm from the center of the reactor. It is worth noting that the length of the plasma column depends on the mean microwave power supplied and the CO_2 inflow rate. The higher the mean power the longer the plasma column that agrees with results obtained at 900 mbar in [40]. At powers of > 2 kW the plasma column length can reach 30–40 cm (see photo in Fig. 3).

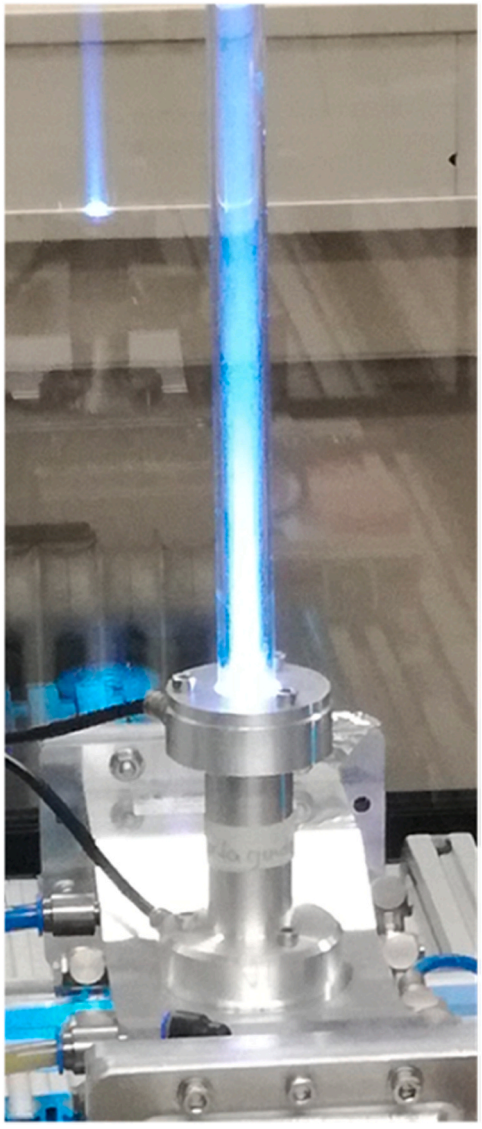


Fig. 3. CO_2 plasma discharge sustained with pulsed microwave in the Surfaguide-based reactor. The CO_2 inflow rate is 15 slm and mean power is 2000 W.

2.3. Plasma torch at IPP with nozzle quenching

Further experiments were conducted with a 2.45 GHz microwave cavity-based plasma torch (see Fig. 4) operated in nozzle configuration. The nozzle configuration was chosen for these experiments as its quick quenching allows to achieve reasonably high energy efficiencies while keeping the effluent at temperatures high enough for waste heat reuse [41]. In another configuration with water-cooled effluent channels even higher CO_2 conversion (up to 57%) could be achieved [16], however at the cost of pushing the effluent temperature down to close to room temperature. The cavity of this microwave plasma torch, which was developed at University of Stuttgart [42,43], consists of a combination of a cylindrical and a coaxial resonator. The plasma torch was operated in the same configuration that was used by R. Antunes et al. [41] in their oxygen separation experiments; that is the plasma was sustained in a flanged quartz tube with an inner diameter of 26 mm above which a water-cooled stainless-steel nozzle that was attached to the plasma reactor. The pressure in the plasma zone was set to 200 mbar for ignition, and was ramped up to 900 mbar immediately afterwards for the actual measurements. After passing through the nozzle, the product gas stream is cooled down to room temperature by flowing through a 2 m long heat exchanger. The composition of the product gas stream was analyzed at the end of the heat exchanger by means of mass spectrometry (see [44] for details on the mass spectrometry system) with an accuracy of ±1.6%. The gas was injected into the reactor via tangential gas inlets at the bottom of the coaxial resonator in order to create a vortex gas flow. Such a swirl gas flow protects the flanged quartz tube from melting by ensuring that the hot plasma gas is surrounded by layers of colder gas. The CO_2 flow rate in all experiments with this setup was set to 7.6 slm (at 25°C) and the pressure inside of the reactor after plasma ignition was kept constant at 900 mbar. At such a quasi-atmospheric pressure, the installation of a nozzle on top of the reactor was demonstrated to drastically enhance conversion and plasma energy efficiency of CO_2 conversion [45]. This performance enhancement is attributed to the quenching of the plasma off-gas imposed by the nozzle, because the hot gas in the center of the plasma reactor is forced to mix with the surrounding layers of colder gas and because of the contact of the hot gas to the water-cooled surfaces of the nozzle [2,45,46]. A microwave source used in actual experiment was the same solid-state microwave generator as one in Surfaguide-based experiment at KIT. A system of WR340 waveguides conducts the microwaves from the generator to the resonant cavity (see diagram at the top of Fig. 4). A manual 3-stub tuner is utilized for impedance matching and power measurements are performed with the use of bi-directional cross-guide coupler and two peak power sensors.

2.4. Methods

2.4.1. Time resolved temperature measurements

In the coaxial torch and Surfaguide-based experiments, for temperature measurements of plasma species, an optical emission spectroscopy (OES) system synchronized with the microwave pulse generator was utilized. The synchronization in coaxial torch experiment was enabled by use of microwave detector measuring the pulse envelope of decoupled incident power [9] and in Surfaguide-based experiments by use of reference TTL pulse signal directly from SSM generator. Precise synchronization (< 1 ns) was achieved by choosing an appropriate delay in the digital delay generator (DDG) and allowed the use of accumulation mode for acquisition of plasma light emission. This significantly increases the signal-to-noise ratio and thus narrows the confidence interval for measured data. The use of the accumulation mode is an essential precondition at low photon's yield in a single acquisition with a short gate time. In iCCD camera Andor A-DH340–18U-03, repetitive acquisitions were summed up (*Integration-on-Chip*) at particular phase of pulse period that allowed to operate the iCCD camera with 50 ns gate. The OES system was wavelength-calibrated using a combined Hg/Ar/Ne

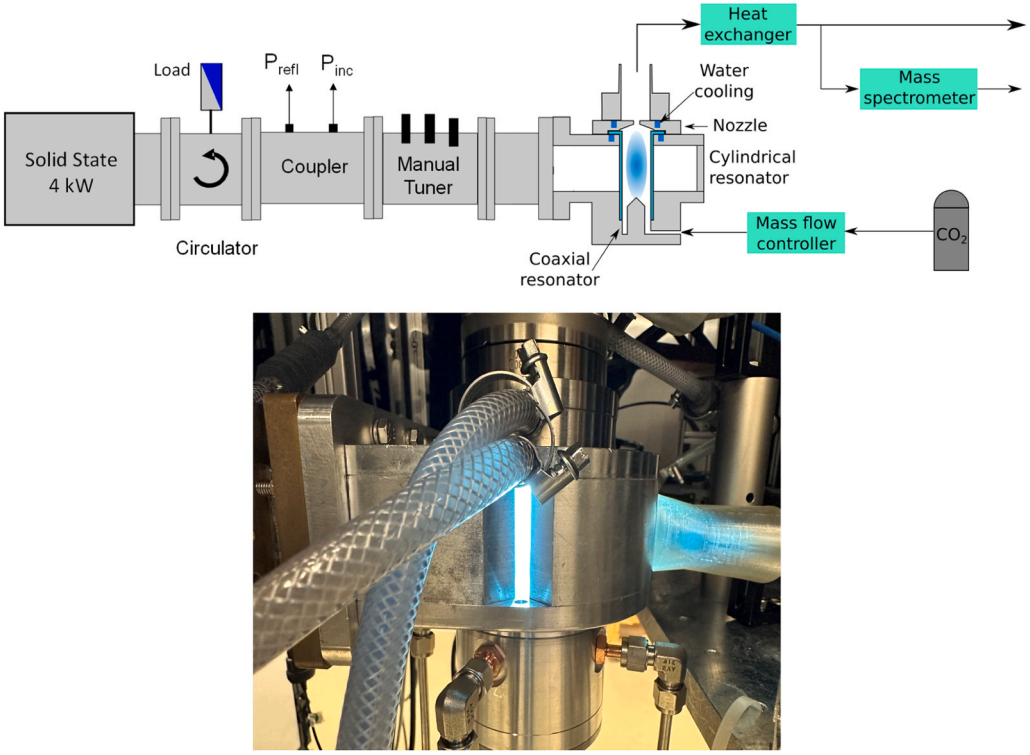


Fig. 4. Plasma torch with the nozzle installed in IPP Garching: (top) schematics of the experiment with microwave and gas supplying and exhaust lines; (bottom) photo of operating torch in CO_2 splitting experiment.

spectral lamp and corrected for the relative spectral response of the optical detection system within the 420–580 nm spectral range. Plasma emission was collected using a collimating lens with an aperture of 4.0 mm. Accordingly, the transverse dimension of the light-collection region was approximately 4.0 mm. In the Surfaguide-based experiment, the collimating lens was mounted in an opening of the side wall of the reactor and aligned such that its line of sight was perpendicular to the reactor tube axis and directed toward the tube center. The collected plasma emission was transmitted through a 2 m optical fiber to the entrance slit of an Acton SP-2756 spectrograph. The rotational and vibrational temperatures were determined by fitting the C_2 Swan emission bands (for T_{rot} >5000 K) and the CO Ångström emission bands (for T_{rot}<5000 K) using the MassiveOES code [47,48]. The rotational temperature is assumed to be representative of the gas temperature due to rapid rotational-to-translational relaxation at atmospheric pressure [10]. It should be noted that the T_{vib} derived from Ångström system corresponds to the vibrational population of the electronically excited $CO(B^1\Sigma^+)$ state. Therefore, it represents an apparent vibrational temperature of the plasma and is used here primarily for comparative analysis between different operating regimes. The systematic error in T_{rot} and T_{vib} is mostly arose from the uncertainty in spectra fitting procedure with MassiveOES, and amounts to 500 K and 1100 K, respectively [10].

2.4.2. Microwave power measurements

The accurate measurement of the absorbed power in the pulsed plasma enables not only the estimation of the process efficiency but also, if they made with sufficient time resolution, a qualitative interpretation of electron density evolution in the discharge [22,25,34,49]. For the evaluation of both incident and reflected power in all three experiments, the real-time power sensors RTP5006 from Boonton Electronics were utilized [50]. These sensors allow to measure the power time profile in RF frequency range 50 MHz to 6 GH with any pulse width > 10 ns and rise/fall time > 3 ns and dynamic range from −50 dBm to + 20 dBm. They feature the N-type 50 Ω input, the external triggering and USB interface. Since the power pulse-form deviates from an ideal rectangular shape (especially in the reflected power signal) the power signals were recorded and integrated with MATLAB software to calculate the mean absorbed power as follows:

$$\overline{P_{abs.pulsed}} = \frac{1}{T}\int_0^T P_{inc}(t)dt - \frac{1}{T}\int_0^T P_{ref}(t)dt \quad (1)$$

Here, $\overline{P_{abs.pulsed}}$ is a mean absorbed power, averaged over an entire period of power pulsation, and P_{inc}, P_{ref} and T are the instant incident and reflected powers and the period of power modulation $T = (t_{on} + t_{off})$, respectively. Note, that due to the group delay dispersion effect the form and effective width of incident pulse is changing while it propagates through the waveguide system and reactor. Therefore, the explicit integration in Eq. 1 provides the correct estimation of mean microwave power in a pulsed regime.

An important parameter of pulsed-power operation is the duty cycle (DC), which characterizes the fraction of time during which microwave power is supplied to the plasma and is defined as

$$DC = t_{on}/(t_{on} + t_{off}). \quad (2)$$

For ideally rectangular incident and reflected power pulses, the mean absorbed power can also be expressed in terms of the duty cycle as:

$$\overline{P_{abs.pulsed}} = DC{\cdot}P_{abs.peak} \quad (3)$$

where, $P_{abs.peak}$ is the peak absorbed power. In the real experimental setup, the pulse waveform is not perfectly rectangular. Therefore, the pulse-on time (t_{on}) and inter-pulse time (t_{off}) are defined as the time intervals between the points at which the microwave power crosses 10% of its peak value.

The leakage of microwave power out the reactor, measured with aid of leakage detector, was always below 1 mW/cm^2 at about 5 cm away from reactor in all experiments. Therefore, it was neglected in the absorbed power estimation.

2.4.3. Measurement of product concentration in afterglow

In the coaxial torch and the Surfaguide-based experiment, effluent gas analysis was enabled with an X-STREAM XEGP gas analyser [51] from Emerson Electric. The gas travelling time from the reactor to the gas detecting sensor amounts ~5 s that enabled an ex-situ monitoring of gas composition versus time with a graphical user interface in the gas analyser. The gas analyser is equipped with detection channels for measuring the volume fractions of CO_2, CO, and O_2 in the effluent gas. The CO and CO_2 channels are based on non-dispersive infrared absorption, whereas the O_2 concentration is measured using a paramagnetic detection principle. In the coaxial-torch and Surfaguide-based experiments, the outlet volume fractions of CO ($y_{CO,out}$), CO_2 ($y_{CO2,out}$) and O_2 ($y_{O2,out}$) were monitored.

In the IPP plasma experiment, the gas composition in the afterglow was analysed with mass spectrometry (MS). The MS system consists of a spectrometer QMG 220 M2 Prisma Plus with cross-beam ion source from Pfeiffer Vacuum. It includes also a custom designed multi-stage gas sampling system enabling measurement of gas compositions over a wide pressure range [44].

2.4.4. Calculation of conversion and energy efficiency

To enable a comparable analysis of the CO_2 splitting performance in the different plasma reactors we calculate the specific energy input (*SEI*) based on the average absorbed microwave power in plasma ($\overline{P_{abs}}$). Note that in pulsed scenarios from Eq. 1. The *SEI* represents a mean amount of energy spent per CO_2 molecule and reads as follows:

$$SEI = \frac{\overline{P_{abs}} \cdot V_m}{F^{in}_{CO2} \cdot N_A}, \tag{4}$$

where F^{in}_{CO2}, V_m, and N_A are the gas inflow rate, molar gas volume (24.47 L/mol) and Avogadro constant, respectively. It should be noted that *SEI* is an average parameter because both absorbed power and axial gas velocity, $v_{gas||}$ (F^{in}_{CO2}=cross-section area [m^2] × $v_{gas||}$ [m/s]) are considered as mean values over the cross-section of the reactor tube. Considering reaction stoichiometry in R1, the CO_2 conversion χ can be calculated from the measured CO volume fraction in the effluent gas ($y_{CO,out}$), as follows [52]:

$$\chi = \frac{y_{CO,\ out}}{1 - y_{CO,\ out}/2} \tag{5}$$

Alternatively, when the measured O_2 volume fraction $y_{O2,out}$ is used, the equivalent expression reads

$$\chi = \frac{2 \cdot y_{O2,\ out}}{1 - y_{O2,\ out}} \tag{6}$$

Both expressions account for the change in the total molar flow resulting from the CO_2 splitting reaction R1. In addition, the energy efficiency of the process is expressed as follows:

$$\eta = \chi \cdot \frac{\Delta H^0_R}{SEI} \tag{7}$$

where ΔH^0_R is the enthalpy of the reaction R1.

3. Results and discussion

3.1. Temperature measurements

Time-resolved plasma-temperature measurements were not available for the cavity-based torch at IPP under pulsed operation. Therefore, no quantitative conclusions regarding the intra-pulse gas-temperature evolution in this reactor are drawn in the present study. For reference, under CW operation, rotational and vibrational temperatures were previously characterized both in the present reactor configuration [46] and with an additional admixer attached to the top of the reactor [53], yielding gas temperatures of approximately 5500–6000 K. These CW values are reported only to characterize the general high-temperature operating regime of the cavity-based torch and are not used as a substitute for the unmeasured pulsed temperature evolution.

3.1.1. Temperature measurements in coaxial torch

For comparison reasons, we summarize in this section the main findings related to temperature measurements in the coaxial torch experiment [9,26]. The microwave power pulsation leads to an effect that the plasma is essentially reignited with each new-coming energy pulse. Consequently, time resolved temperature measurements using optical emission spectroscopy (OES) were only possible during the microwave pulse and shortly thereafter, until the excited molecular states faded. The main finding is the discovery of nonequilibrium plasma state with $T_{vib}/T_{rot} \approx 2$ in the beginning of the pulse, provided the pulse time $t_{on} \geq 1.5$ μs (see Fig. 10 in [26]). During the pulse, the rotational temperature rises nonlinearly from its initial value – typically between 3000 K and 4000 K – until it approaches the vibrational temperature, which spans between 7000 K and 8000 K. Once VT equilibrium is reached, both temperatures remain nearly constant throughout the remainder of the pulse and decrease rapidly after the pulse-end. It is worth noting that, that the increase of T_{vib} in the beginning of pulse is not resolved within the 50 ns time resolution, therefore the e-V energy transfer is supposed to be faster than 50 ns. It is insightful that the time required for the thermalization is not constant but rather depends on pulsation timing. For scenarios with the same t_{on}= 2.5 μs T_{rot} recovers earlier in the scenario with shorter inter-pulse time t_{off}= 3.75 μs as compared with scenario with longer t_{off}= 7.5 μs (Fig. 9 in [26]). The found approximate thermalization times of 800 ns (at t_{off}=3.75 μs) and 1600 ns (at t_{off}=7.5 μs) are at least in the same order of magnitude as the predicted VT relaxation time in [54]: for a given pressure and 3000 <T_g< 7000 K, it spans between 300 and 800 ns. As to the temperature decrease after pulse-end, the detection of the excited C_2 rovibrational bands was restricted because of their relative quick fading. Note, the period after pulse-end when the OES can still resolve reducing signal above the noise level indirectly reflects the rate of temperature decrease, and depends on pulsing scenario. It is hard to make a strong conclusion how the rate of energy dissipation from plasma is linked to the pulsation timing. Nonetheless, for two scenarios with the same t_{on} (=2.5 μs), there is a hint that the cooling rate is lower for the scenario with a shorter t_{off} (=3.75 μs) as compared with one with a longer t_{off} (=7.5 μs); it is also indirectly confirmed by a shorter period detectability of excited bands after pulse-end: 650 ns and 1050 ns respectively (Fig. 9 in [26]).

3.1.2. Temperature measurements in the surfaguide-based reactor

In the Surfaguide-based reactor, energy coupling, plasma confinement, and gas flow configuration differ from those in the coaxial plasma torch. The plasma was sustained within a quartz dielectric tube which transverses the reactor, that results in a significantly larger plasma–microwave interaction volume as compared with the coaxial setup. This extended interaction region together with the efficient waveguide-based power delivery, enables plasma operation at kilowatt power levels. Plasma temperatures were investigated in four pulse scenarios with the peak power at 4.2 kW and varied duration of pulse (t_{on}) and inter-pulse (t_{off}) times, as listed in Table 2. Additionally, for every pulsed scenario the reference CW power scenario was performed in such a way that a mean absorbed power both in CW and pulsed regimes were approximately equal – $P_{abs,CW} \approx \overline{P_{abs,pulsed}}$ – their deviation is indicated in the last column of Table 2.

In the Surfaguide-based experiment, it was empirically determined that, at a peak power of 4.2 kW, stable plasma operation could only be sustained for t_{off} < 12 μs. For longer t_{off} the plasma extinguishes. In addition, a lower limit of approximately 700 W was identified for the mean absorbed microwave power required to sustain the discharge in

Table 2
Pulse scenarios for Surfaguide-based reactor with different t_{on} and t_{off} times, peak power of 4.2 kW, CO_2 inflow of 15 slm and atmospheric pressure. Mean absorbed power deviation from corresponding reference (CW) scenario is indicated in the last column.

Scenario	t_{on}	t_{off}	DC	$\overline{P_{abs.pulsed}}$	Deviation compared to CW
1	0.2 μs	0.8 μs	0.20	0.75 kW	±0.02 kW
2	5.0 μs	5.0 μs	0.50	1.88 kW	±0.10 kW
3	5.0 μs	10.0 μs	0.33	1.26 kW	±0.10 kW
4	10.0 μs	10.0 μs	0.50	1.84 kW	±0.10 kW

the present setup. For each pulsed scenario, time-resolved measurements of the vibrational (T_{vib}) and rotational (T_{rot}) temperatures were performed. In the reference CW operation, the temperatures were measured in a non-time-resolved manner using the same OES procedure as for the pulsed plasmas. The results are summarized in Fig. 5, where the shaded areas around the data points represent systematic uncertainties arising from OES spectral fitting in MassiveOES [10] and temperatures in CW scenarios are shown as horizontal bars. In scenarios 1 and 3, finer temporal resolution was employed in an attempt to resolve fast temperature dynamics. However, the measured temperature traces exhibited relatively smooth temporal behavior for both T_{vib} and T_{rot}. Consequently, coarser time steps were chosen for scenarios 2 and 4.

In pulsed microwave plasma, the important difference between the Surfaguide-based and coaxial torch experiments is that the plasma in the Surfaguide-based reactor does not extinguish between microwave pulses and therefore no reignition phenomenon occurs. Plasma, at least in the center of the Surfaguide-based reactor, exists both during power-ON and power-OFF time intervals. The evidence for that is the fact that the rotational C_2 Swan emission bands, which were used to derive plasma temperatures, are well detectable both in and out of microwave pulse. As a reference, temperatures measured in CW discharges operated at the same average microwave power as in each pulsed scenario are indicated by horizontal bars. A common trend observed for both rotational and vibrational temperature traces is an increase during the microwave pulse and a decrease during the inter-pulse period. This behavior qualitatively agrees with coaxial torch results [26], although the modulation of T_{rot} in the coaxial torch was significantly larger - reaching up to 3500 K due to the reignition phenomenon. In the absence of reignition and depending on the discharge conditions, the amplitude of temperature modulation is the smallest in scenario 1 (=100 K, Fig. 5a) and the biggest in scenario 3 (=500 K, Fig. 5c). Although the magnitude of the temperature modulation lies within the systematic error bars of the diagnostic, its presence is found to be statistically significant and phase-locked to the imposed power modulation [55,56]. In that case, the systematic errors are not representative in the case when the parameters for spectra fitting (main contributor to above systematic error) are kept unchanged throughout all measured time points. In scenario 3, with t_{on} = 5.0 μs, t_{off} = 10.0 μs, the temperature modulation is found at most pronounced. Importantly, the amplitude of temperature modulation depends on t_{off} – compare the scenario 2 and 3 with the same t_{on} = 5.0 μs. The longer the inter-pulse time the bigger increase of temperature during power-on phase. The same is valid for scenarios 2 and 4 with the same DC (mean power) but different t_{on}/t_{off} timings: 5.0 μs/5.0 μs (scenario 2) against 10.0 μs/10.0 μs (scenario 4). The longer power-off time in scenario 4 results in larger temperature modulation. Since temperature modulation occurs on top of the reference CW temperature level, the mean gas temperature in the pulsed regime is higher than that observed under CW operation. It is highly unlikely that the higher microwave power applied at flat-top of the pulse (4.2 kW) as compared with CW microwave power may result in an increase in plasma temperature during power-on phase. In accordance with results obtained by E. Carbone et al. [10] where CW power was scanned between 0.9 kW and 2.7 kW and CO_2 plasma sustained at 0.925 bar pressure, the rotational temperature was about 6000 K independent on the supplied

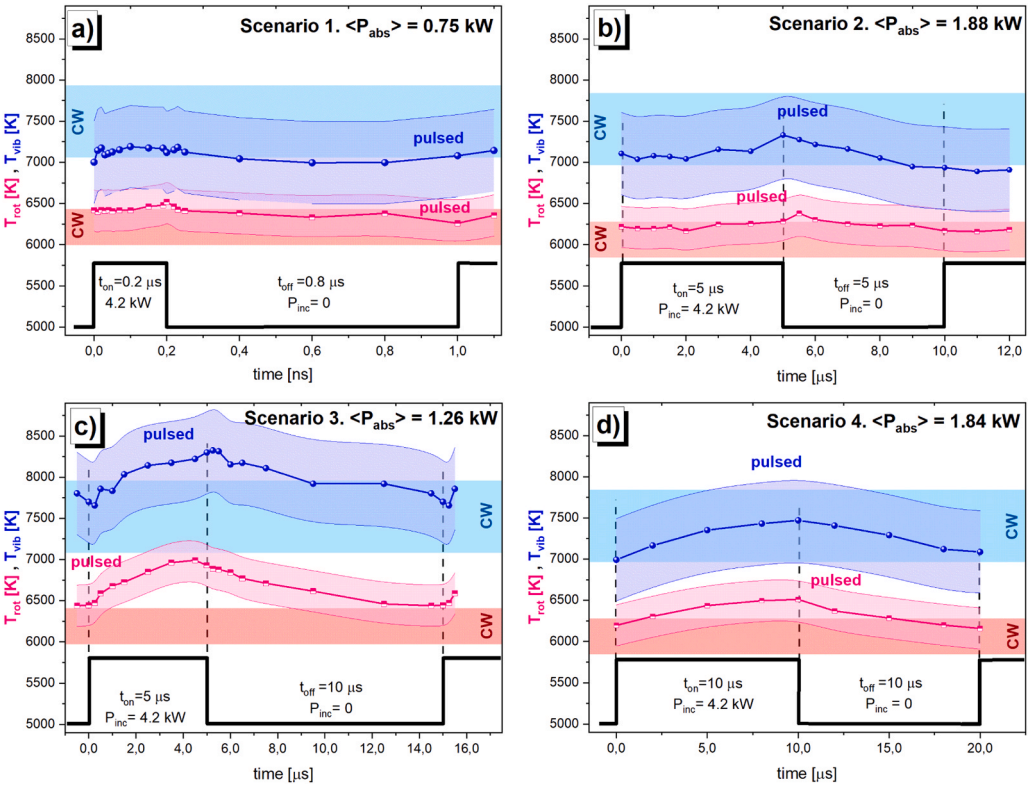


Fig. 5. Rotational and vibrational temperatures measured in Surfaguide-based reactor for scenarios 1–4 listed in Table 2 with different t_{on} and t_{off} times. Results for CW scenarios are shown with horizontal light red and blue bars as a reference. Thick black lines sketch the timing for microwave power pulsations. Confidence intervals of 500K for T_{rot} and 1100K for T_{vib} are shown as shaded areas for both the CW and pulsed data.

power. Our T_{rot} data in CW scenarios with different microwave powers depicted in Fig. 5 also shows nearly constant temperature of about 6300 K.

A possible explanation for the observed T_{rot} and T_{vib} variations may involve the transient response of the electron component to microwave power modulation, as observed by time-resolved Thomson scattering in other pulsed plasmas [20,30]). Following microwave power termination, both the electron density and electron temperature can decrease, with T_e typically responding on a shorter timescale than n_e [20,30]. Consequently, the electron population and energy distribution at the beginning of the subsequent microwave pulse may differ from those under steady-state CW conditions. Since the rate coefficients of electron-impact processes depend strongly and nonlinearly on the electron energy distribution, such transient conditions may alter the partitioning of absorbed microwave energy among vibrational and electronic excitation, dissociation, and gas heating [18,20,31]. Vibrational excitation followed by V–T relaxation, together with quenching of electronically excited states, provides pathways for transferring part of the deposited energy to translational degrees of freedom and may therefore contribute to the observed modulation of T_{rot} and T_{vib}. However, n_e(t) and T_e(t) and the EEDF were not measured in the present experiments; therefore, this mechanism is proposed as a possible interpretation rather than a direct experimental conclusion.

The relaxation of T_{rot} after end of pulse (~5E7 K/s in scenario 3) is quite decent as compared to required rate for ideal quenching of 1E8 K/s [11] but significantly slower than the rate of ~2E9 K/s observed in the coaxial torch experiment. The most likely physical mechanism underlying this difference is significantly different convective heat transport in the two reactor configurations. In the coaxial torch, the plasma plume expands directly into the exhaust glass tube of substantially larger cross section, which promotes rapid mixing with the surrounding colder gas and enhances convective cooling. In contrast, in the Surfaguide-based reactor, the hot afterglow remains confined within the extended quartz tube, resulting in a slower heat removal and a correspondingly slower decay of the rotational temperature.

For estimated ~5E7 K/s relaxation rate and assuming linear decrease, the cooling down to approximately 3000 K (the inter-pulse temperature in coaxial torch [26]) would require an inter-pulse duration of several tens of microseconds. Yet, such long inter-pulse durations were not achievable in present configuration.

3.2. Conversion and energy efficiency

3.2.1. Conversion and efficiency in the coaxial torch

As a reference, we present in this section a short summary of the results obtained in the coaxial plasma torch experiment published in [9, 26]. Estimation of conversion and energy efficiency for reaction R1 in the coaxial torch experiment demonstrated that the pulsed plasma regime outperforms the CW mode by a factor of two [9,26]. The overall performance for all regimes with different pulsation times is presented as color-coded 2D plot in Fig. 6, where efficiency (η) is plotted over conversion (χ), and symbol's color represents specific energy input (*SEI*). The conversion values originally reported in [9] were evaluated from the measured O_2 volume fraction using the approximation $\chi \approx 2{\cdot}y_{O2,out}$. For the present comparison, the original data were recalculated using the exact expression given in Eq. (6). The resulting correction is below 0.62% for all data points; the corresponding energy efficiency values were corrected by the same relative amount. Data points corresponding to pulsed scenarios with the same t_{on} time and different t_{off} times are indicated by the same symbols. Reference CW scenarios are depicted using spherical markers. The point-to-point measurement uncertainty was estimated using repeated acquisitions and amounts to ±0.1% in conversion and ±0.7% in efficiency. The hatched black and red areas indicate the ranges in (χ,η)-space accessible in both CW and pulsed operation respectively. The dashed lines guide the linear dependence of η on χ at fixed *SEI* that agrees with Eq. 7. More details on that experiment can be found in [9,26]. The main result of that experiment is that microwave power pulsation more than doubled both χ and η relative to the corresponding CW values at comparable *SEI*.

3.2.2. Conversion and efficiency in the surfaguide-based reactor

In this conversion and efficiency estimation experiment using the

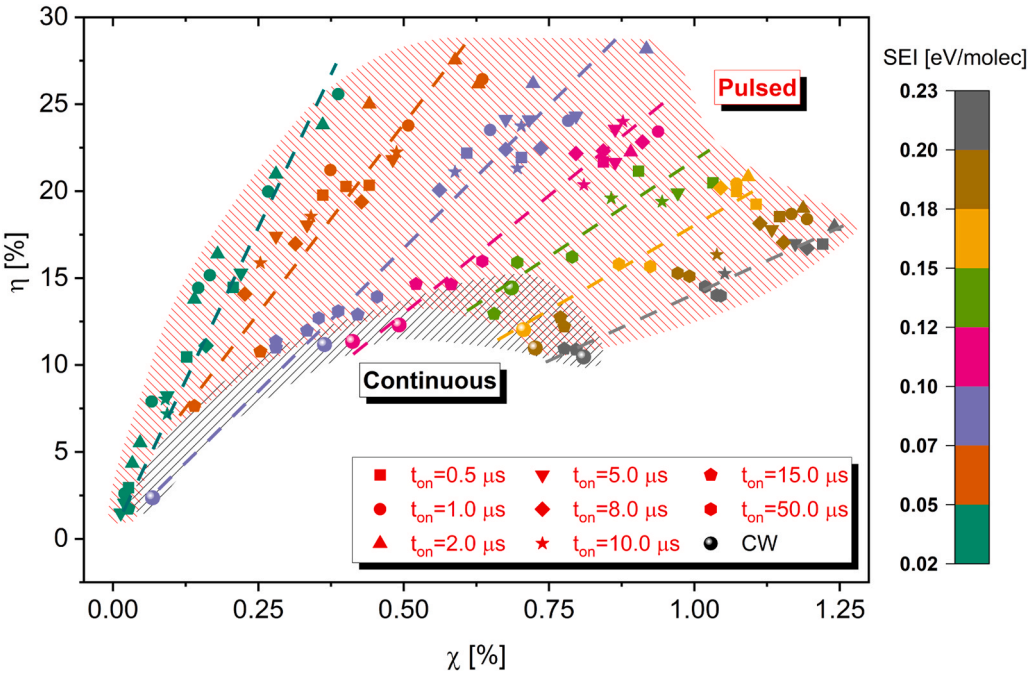


Fig. 6. Energy efficiency (η) vs conversion (χ) for pulsed and continuous wave (CW) plasma scenarios of CO_2 conversion in the coaxial torch. CW data are shown with spheres. Pulsed microwave data for different t_{on} times (indicated on graph) are presented with different symbols accordingly. Hatched black and red areas indicate the ranges in (χ,η)-space accessible in CW and pulsed scenarios respectively. *SEI* is colour coded. Dashed lines guide the points with *SEI*=const, which agrees with linear $\eta(\chi)$ dependency according to Eq. 7. Point-to-point measurement uncertainty in conversion and efficiency amount to ±0.1% and ±0.7%, respectively.

Surfaguide-based reactor, the peak power and CO_2 inflow rate were kept constant at 3.0 kW and 15 slm, respectively. The pulse time (t_{on}) was varied from 1.0 μs to 7.5 μs. And for every fixed t_{on}, the t_{off} time was varied gradually from smallest value up to the largest possible value while keeping minimum mean supplied power > 700 W. For a given variations of t_{on} and t_{off} times, the *SEI* for all regimes spans within 0.7–2.7 eV/molecule. The obtained conversion and energy efficiency data were compared against reference CW plasmas sustained with different power levels (see Figs. 7a and 7b). The data are plotted versus *SEI* and absorbed power for convenience, with different symbols for every fixed t_{on} regime. The CW data are represented by black squares and highlighted with black hatched area in Fig. 7a and b. The point-to-point measurement uncertainty was estimated using repeated acquisitions and amounts to ±0.2% in conversion and ±0.7% in efficiency. It is worth noting, that regimes with $t_{on} = 1$ μs and 2 μs reveal only minor improvements as compared with CW scenarios. The scenarios with $t_{on} \geq 4$ μs show remarkable progress in the reactor performance (highlighted with red hatched area). In all pulsed regimes, the maximum relative gains in conversion and efficiency compared to the corresponding CW values reach 36% and 30%, respectively, within the *SEI* range of 1.3–2.0 eV/molecule. The maximum absolute conversion and efficiency achieved under pulsed regimes reach 15% and 30%, respectively. In Fig. 8, the $\chi(SEI)$ and $\eta(SEI)$ dependencies are summarized in one (χ,η) color-coded plot. Scenarios with different t_{on} times are shown with different symbols and *SEI* is color coded. The hatched black and red areas indicate the range in (χ,η)-space accessible in CW and pulsed scenarios respectively. The dashed straight lines for fixed *SEI* guide the eye to elucidate the linear dependence of η on χ that agrees with Eq. 6. The observed overall progress in pulsing regimes is smaller than one observed in coaxial torch, where relative increase amounted to ≥ 100% (see Fig. 6). Yet, the geometry of the two experiments and the *SEI* range are also quite different. In the coaxial torch the observed improvements referred to non-equilibrium states in the beginning of the pulse, reignition phenomenon and plasma volume increase, while in the Surfaguide-based, T_{rot} and T_{vib} are close to each other and are modulated not so significantly as in the coaxial torch.

The observed difference in relative performance enhancement under pulsed operation between the Surfaguide-based reactor and the coaxial torch may be partly related to the markedly different gas-temperature modulation in the two systems. In the coaxial-torch experiment, T_{rot} varied between approximately 3000 and 7000 K over the pulsation cycle (Fig. 3 in [9]), whereas the increase in gas temperature under pulsed operation relative to CW operation in the Surfaguide-based reactor is moderate (<500 K; best-performing scenario shown in Fig. 5c). During the power-OFF phase T_{rot} does not decrease below approximately

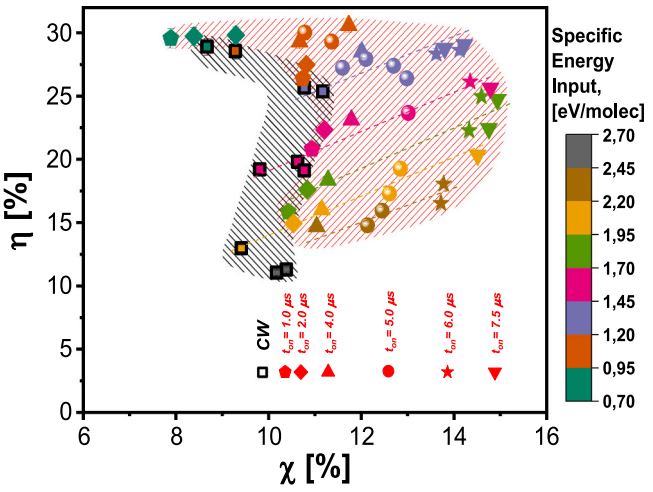


Fig. 8. Energy efficiency versus conversion for CO_2 splitting in Surfaguide-based reactor for investigated regimes. Continuous wave (CW) data are shown with squares. Pulsed data for different t_{on} times (indicated on graph) are presented with different symbols accordingly. Colour coding corresponds to specific energy input (*SEI*). Hatched black and red areas highlight assessed (χ,η) regions in CW and pulsed regimes respectively. Dashed lines guide the points with *SEI*=const, which agrees with linear $\eta(\chi)$ dependency according to Eq. 7. Point-to-point measurement uncertainty in conversion is ±0.2% and in efficiency ±0.7%.

6000–6500 K, resulting in a full excursion between approximately 6500 and 7000 K. To quantify the direct influence of these experimentally observed gas-temperature variations on thermal CO_2 chemistry, the temperature dependence of the principal CO_2 dissociation and CO_2-forming back reactions was evaluated using the Arrhenius rate coefficients reported by Vermeiren and Bogaerts [57]: $k_i = A_i e^{-T_{a,i}/T_g}$, where, A_i is the pre-exponential factor and $T_{a,i}$ is activation temperature. In addition to the two CO_2-forming back reactions R2 and R3 introduced in Section 1, the following CO_2 dissociation reactions were considered:

$$CO_2 + M \rightarrow CO + O + M \quad \text{(R4)}$$

$$CO_2 + O \rightarrow CO + O_2 \quad \text{(R5)}$$

where M denotes a third-body collision partner. To characterize the temperature sensitivity of each reaction over the experimentally relevant temperature intervals, the rate-coefficient ratio S_i was defined as $S_i = k_i(T_{g,\max})/k_i(T_{g,\min})$. The kinetic parameters and the corresponding

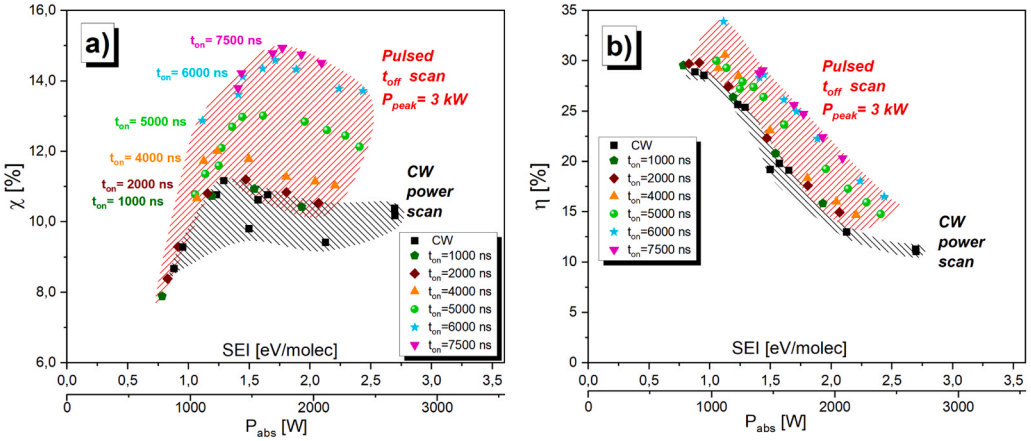


Fig. 7. a) $\chi(SEI)$ and b) $\eta(SEI)$ for plasmas in the Surfaguide-based reactor. Continuous wave (CW) data are shown with closed black squares as reference. Pulsed data for different t_{on} times (indicated on graph) are presented with different symbols accordingly. Hatched black and red areas highlight assessed (χ,η) regions in CW and pulsed regimes respectively. Point-to-point measurement uncertainty in conversion is ±0.2% and in efficiency ±0.7%.

S_i factors for coaxial torch and Surfaguide-based reactor experiments are summarized in Table 3.

As shown in Table 3, this strongly suppresses the thermal dissociation rate coefficients (R4 and R5), while the CO_2-forming back reactions exhibit weaker temperature dependence. Rapid cooling therefore reduces the overall thermal chemical activity after termination of the microwave power and, together with the evolving species composition and transport, may contribute to limiting post-discharge back reactions and preserving the dissociation products.

In contrast, the plasma in the Surfaguide-based reactor does not extinguish between microwave pulses, and the increased T_g under pulsed operation may favor thermal CO_2 dissociation: over the measured 6500–7000 K range, the most temperature-sensitive dissociation pathway R4 changes by a factor of 1.78, compared with only 1.02 and 1.18 for the back reactions R2 and R3, respectively. This preferential temperature sensitivity may contribute to the observed increase in CO_2 conversion under pulsed operation. It should be emphasized that the factors S_i characterize only the temperature dependence of the elementary rate coefficients and not the corresponding volumetric reaction rates, which additionally depend on the time-dependent local species densities.

3.2.3. Conversion and efficiency in the IPP plasma experiment

In this section, we report on the CO_2 conversion and energy efficiency in the third investigated plasma reactor where pulsed microwave power was applied. Among all three considered configurations, only the plasma torch installed at IPP is equipped with an active gas temperature quenching in the reactor afterglow. As in the two other reactors, we have used also here the continuous wave (CW) scenario as a reference to elucidate the changes in conversion and efficiency of the process when CW is replaced with pulsed energy supply.

For variation of specific energy input we have varied 1) the microwave input power in the CW scenario, 2) the inter-pulse time, t_{off}, at fixed t_{on} time in the pulsed scenario. The following t_{on} pulse times were considered: 1.0 μs and 4 μs. Note, because of lower CO_2 input flow (7.6 slm) than one in the Surfaguide-based experiment, the *SEI* spans from 1.5 to 5.0 eV/molecule, while in the Surfaguide-based experiment it was within 0.7 – 2.7 eV/molecule. The results are summarized in Fig. 9 where the conversion and efficiency are plotted against *SEI* and mean absorbed microwave power (P_{abs}).

Additionally, the symbols are filled with colors, that are coded according to the duty cycle (*DC*) values which are proportional to the mean supplied power. Note that at higher CW powers (correspond to higher *SEI* on that graphs), the cooling power of one chiller was not enough and two chillers in parallel were utilized – see blue and black circles in Fig. 9.

Table 3
Arrhenius parameters for thermal CO_2 dissociation and CO_2-forming back reactions R2–R5 [57], and corresponding rate-coefficient ratios $S_i = k_i(T_{g,\max})/k_i(T_{g,\min})$ over the experimentally relevant temperature intervals in coaxial torch and Surfaguide-based reactor.

CO_2 Reactions		A_i	$T_{a,i}$ (K)	S_i	
				Coaxial torch 7000/3000 K	Surfaguide 7000/6500 K
Back reactions	R2[a]	8.3×10^{-46} m^6s^{-1}	1510 K	1.3	1.02
	R3	3.99×10^{-20} m^3s^{-1}	15275 K	18	1.18
Dissociation	R4	6.06×10^{-16} m^3s^{-1}	52525 K	2×10^4	1.78
	R5	7.95×10^{-18} m^3s^{-1}	18161 K	32	1.22

[a] For R2, the collider-dependent multiplicative factors reported in Ref. [57] do not affect S_2, because they cancel in the rate-coefficient ratio.

Qualitatively, the conversion has the similar peaked behavior as in the Surfaguide-based experiment (see Fig. 7a) – yet, the peak is at around 3.5 eV/molecule while the maximum in the Surfaguide-based data, depending on pulsation regime, lies between 1.24 and 1.80 eV/molecule. Notably, no difference between CW and pulsed data as well as between two pulsation regimes is detected. Similar to the Surfaguide-based experiment, energy efficiency demonstrates the same falling trend along with the *SEI*. Also here, no difference between pulsed and CW regimes is found (Fig. 9b). In the next experiment, to investigate the pulsed regime in a broader parameter range, we have varied both t_{on} and t_{off} times but keeping duty cycle constant ($DC \approx 0.437$) that corresponds to $SEI = 3.5$ eV/molecule where maximum in $\chi(SEI)$ data is detected. The resulting conversion and energy efficiency are plotted in Fig. 10 versus t_{on} time [53]. Note, as the *DC* was fixed, the progression along t_{on} axis corresponds to an increase in the corresponding t_{off} values. The obtained data, also here, show no difference between CW and pulsed data within the confidence interval. Also, no dependency on t_{on} (correspondingly t_{off}) time was found both for conversion and efficiency. It is worth noting that at all experiments with a given peak power of about 4 kW, the maximum t_{off} time when plasma was relatively stable was up to 10.3 μs. At longer t_{off} times, plasma became unstable and these results are not analyzed in present paper. At the same time, the found limit is close to maximum $t_{off} = 12$ μs, observed in the Surfaguide-based experiment.

A possible explanation for the different response to microwave power pulsation in the two kW-scale reactors lies in their substantially different post-plasma treatment. In the Surfaguide-based reactor, pulsed operation produces a measurable enhancement relative to the corresponding CW operation, whereas no such enhancement is observed in the cavity-based torch at IPP. The latter is equipped with a water-cooled quenching nozzle immediately downstream of the plasma region. The effect of this nozzle on the downstream thermal field has been investigated experimentally and numerically in the same reactor configuration [46]. The nozzle strongly shortens the hot afterglow by promoting mixing between the hot central gas and colder peripheral gas and by heat transfer to the water-cooled nozzle walls [46]. By comparing the conversion in CW operation for $SEI \approx 2$ eV/molecule in Fig. 7a and 9 a we may see that the rapid quenching in the plasma torch at IPP nearly doubles the conversion from ≈ 9% to ≈ 17%.

In the Surfaguide-based experiment, the gas quenching is rather weak and slow. Effectively, the hot region where the dissociation reactions take place is extended into after-reactor zone. It can be evident also from visual observation of plasma in Surfaguide-based reactor in Fig. 3 where bright, intense light emitting plasma area expands a lot above the reactor. In modelling work of V. Vermeiren and A. Bogaerts it is shown that especially for high *SEI* when the residence reactor time is relatively short, the temperature and the conversion may continue to rise in the afterglow region [57]. We suppose that plasma in the Surfaguide-based reactor takes maximum advantage from the increase of gas temperature in the pulsed regime due to its extended effective residence time (slow and late quenching) as compared to IPP experiment. In the same work V. Vermeiren and A. Bogaerts have shown, that the earlier quenching, before maximum conversion is reached, can be counter-productive [58]. In summary, the system with very fast and massive quenching in the water-cooled nozzle as in the plasma torch at IPP, apparently, cannot benefit from pulsation scenario because of its shorter effective residence time, as compared with the Surfaguide-based reactor under consideration.

3.3. Reflected power as a monitor for electron density

In this chapter, we consider how the reflected power signal can be related to the dynamics of electron density in power pulsation scenarios. The time-averaged electromagnetic power absorption density (Joule dissipation) in a conductive medium reads as follows:

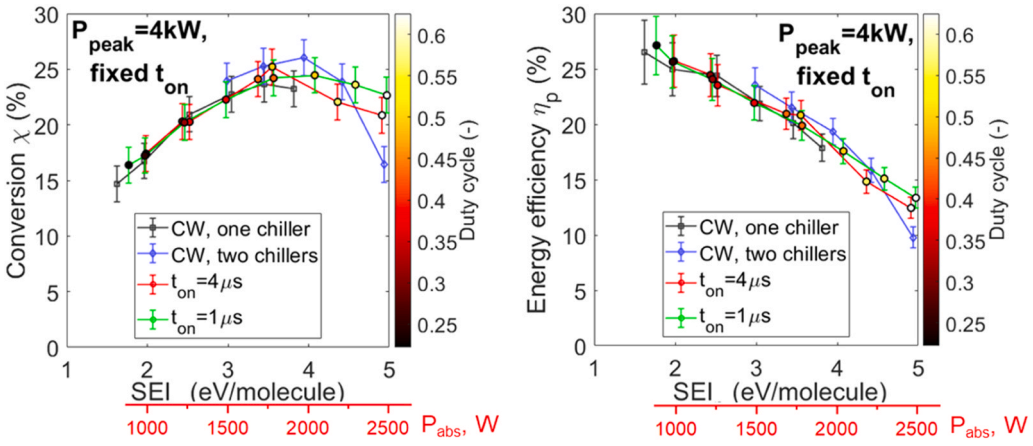


Fig. 9. Plasma torch at IPP: (a) CO_2 conversion vs *SEI* and absorbed microwave power. Continuous wave (CW) data shown with blue and black lines. Pulsed microwave data for t_{on} = 1 μs and 4 μs are presented with green and red. Parameters: p = 0.9 bar, F_{CO2}= 7.6 slm, P_{peak}= 4 KW, D_{in}= 26 mm.

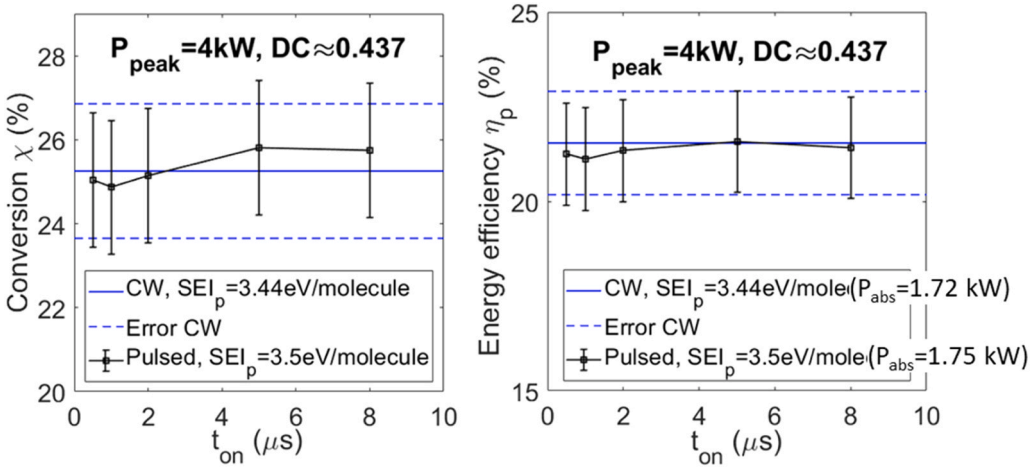


Fig. 10. Plasma torch installed at IPP. Energy efficiency and conversion for different pulse times (t_{on}) at fixed DC= 0.437 [55].

$$p_{abs} = \frac{1}{2}\cdot \mathrm{Re}[\sigma]\cdot |E|^2 \tag{8}$$

where σ and E are the conductivity of the plasma and the electric field of microwave. For harmonically oscillating electric field with angular frequency ω, the conductivity of cold collision plasma is expressed as follows [59]:

$$\sigma = \frac{e^2\cdot n_e}{m_e\cdot(\nu_{en} - i\cdot\omega)} \tag{9}$$

where n_e, e, and ν_{en} are electron density, electron charge and electron-neutral collision frequency. From Eqs. 8 and 9, it results in:

$$p_{abs} = \frac{1}{2}\cdot\frac{e^2\cdot n_e\cdot\nu_{en}}{m_e\cdot(\nu_{en}^2 + \omega^2)}\cdot|E|^2 \tag{10}$$

Assuming Maxwellian electron energy distribution function with electron temperature T_e, the electron-neutral particle collision frequency can be expressed as follows [60]:

$$\nu_{en}(t) = n_n\cdot\overline{\sigma_{mt}}(T_e)\cdot\sqrt{\frac{8\cdot k_B\cdot T_e}{\pi\cdot m_e}} \tag{11}$$

where n_n, $\overline{\sigma_{mt}}(T_e)$ and k_B are neutral particle density, mean cross section of electron momentum transfer (which depends on T_e) and Boltzmann constant respectively. To make a transition to a full absorbed power, one needs to integrate Eq. 9 over the volume where the microwave field is coupled into the plasma. It is worth noting that, due to differences in microwave-to-plasma coupling between the coaxial torch and the two kilowatt-scale reactor configurations, the volume in which the incident electric field interacts with plasma electrons can differ substantially. In the coaxial torch, this interaction volume is geometrically confined to the region between the inner and outer electrodes near the torch exit. In contrast, the Surfaguide-based reactor and the cavity-based torch provide a significantly larger interaction volume owing to the electric field orientation and the larger spatial overlap between the microwave field and the flowing plasma-forming gas. Additionally, considering a maximum electron density of approximately 1×10^{19} m^{-3} for given plasma conditions [61] together with the electron-neutral collision rate at atmospheric pressure, the estimated microwave penetration depth at 2.45 GHz is on the order of 10 mm. This indicates, that plasma can be treated like effectively transparent lossy medium and the integration over the volume is well justified. Accordingly, temporal variations in the spatial distributions of the electron density n_e and electron temperature T_e are assumed to be less significant than the evolution of their volume-averaged values, defined as: $\langle n_e\rangle(t) = \frac{1}{V}\int_V n_e(x,y,z,t)$ and $\langle T_e\rangle(t) = \frac{1}{V}\int_V T_e(x,y,z,t)$. In addition, we define the volume-integrated electric field energy as follows: $W_E(t) = \frac{1}{2}\int_V |E(x,y,z,t)|^2$. Under these approximations, and considering that the electron-neutral collision frequency significantly exceeds the microwave angular frequency ($\nu_{en}\gg\omega$) at 2.45 GHz, the Eq. 10 can be reformulated to express the

instantaneous absorbed power as:

$$P_{abs}(t) = \frac{e^2}{m_e}\cdot\frac{\langle n_e\rangle(t)}{\langle \nu_{en}\rangle(t)}\cdot W_E(t) \quad (12)$$

where the effective electron-neutral collision frequency is given by $\langle \nu_{en}\rangle(t) = n_n(t)\cdot\overline{\sigma_{mt}}(\langle T_e\rangle(t))\cdot\sqrt{\frac{8\cdot k_B\cdot\langle T_e\rangle(t)}{\pi\cdot m_e}}$. Here, the neutral density $n_n(t)$, because of weak pressure variations, is primarily governed by the gas temperature ($n_n \sim 1/T_{gas}$) whereas the mean cross-section for momentum transfer $\overline{\sigma_{mt}}$ can vary significantly as the mean electron temperature $\langle T_e\rangle(t)$ is expected to be modulated significantly along with modulated MW power. As a discharge volume and microwave coupling efficiency are time dependent, the variation of electric field energy integral $W_E(t)$ can also contribute to the overall absorbed power. Taking these effects into account, the instantaneous reflected power can be expressed as:

$$P_{ref}(t) = P_{inc}(t) - \frac{e^2}{m_e}\cdot\frac{\langle n_e\rangle(t)}{\langle \nu_{en}\rangle(t)}\cdot W_E(t) \quad (13)$$

Since the incident power $P_{inc}(t)$ is known, and the effective electron-neutral collision frequency $\langle \nu_{en}\rangle(t)$ and the electric field integral $W_E(t)$ can be estimated, Eq. 13 provides a relationship between measured reflected power $P_{ref}(t)$ and volume-averaged electron density $\langle n_e\rangle(t)$. It is worth noting that variations in electron density may correlate with variations in $P_{ref}(t)$, but cannot be uniquely inferred from it. Nevertheless, the reflected power signal enables a qualitative interpretation of $\langle n_e\rangle(t)$. In future, the quantitative n_e analysis might be also possible by accounting the complex reflection coefficient and varying the n_e profile how it was realized in [62] or via optical emission spectroscopy using Stark broadening of Ar I lines.

In the following two sections, the behavior of the reflected microwave power signal is compared for two distinct regimes: one exhibiting plasma reignition (as observed in the coaxial torch reference case) and one without reignition (as in the Surfaguide-based and cavity-based plasma torches). It will be shown that, in addition to plasma temperature, the reflected power signal can serve as a sensitive qualitative indicator of the temporal evolution of plasma electron density.

3.3.1. *Reflected power in coaxial torch experiment*

As a baseline for comparison with the two kilowatt-range microwave experiments, this section examines the temporal behavior of the reflected power in the coaxial plasma torch operated under pulsed conditions. In this reference case, the CO_2 flow rate was 12 slm, while the peak microwave power was limited to 250 W. It should be noted that the impedance of the transmission lines – both between the microwave source and the plasma, and between the source and the power detectors – was kept constant throughout the experiments. Therefore, any observed impedance mismatch can be attributed solely to changes in plasma properties. Fig. 11 presents the reflected power signals for three discharge conditions with identical pulse duration (t_{on} =2.0 μs) but different inter-pulse times (t_{off} =12.0, 6.0 and 1.5 μs). All traces exhibit a pronounced peak at the beginning of each pulse. This initial peak in reflected power (Fig. 11 b) reflects a transient competition between the rapidly rising incident power (due to the initial impedance mismatch) and the nascent plasma whose volume [9] and $\langle n_e\rangle$ increase over time. In other words, the simultaneous increase in $\langle n_e\rangle$ and in the factor W_E (associated with the expanding discharge volume and improving microwave coupling) leads to a progressive rise in the plasma absorption capability. According to Eq. 12 this absorption scales as $\langle n_e\rangle(t)/\langle \nu_{en}\rangle(t)\cdot W_E(t)$ and once it becomes comparable to or exceeds $P_{\mathrm{inc}}(t)$, a corresponding decrease in the reflected power is observed. Thus, in the reignition regime, the characteristic peak structure in the reflected power arises from the temporal interplay between the rising pulse profile of $P_{\mathrm{inc}}(t)$ and the increasing absorption capacity of the developing plasma. The difference in timing and amplitude of the observed maxima for different inter-pulse times (see Fig. 11 b) can be attributed to variations in seed ionization, which seems to be the lowest for the longest inter-pulse time t_{off}. Correspondingly, the lower rate of seed ionization leads to a later breakdown and slower plasma development, that makes the first term in Eq. 13 more dominating and leading to a peak with higher amplitude and later time coordinate: 21 ns, 23 ns and 30 ns for t_{off} = 1.5 us, 6.0 μs and 12.0 μs respectively. As to dependence of power absorption on electron-neutral collision frequency, it scales with electron and gas temperatures as $1/T_{gas}\cdot\overline{\sigma_{mt}}(T_e)\cdot\sqrt{T_e}$ (see Eq. 12). The time scale for T_{gas} is much slower than rising time of microwave therefore T_{gas} in the beginning of pulse can be considered nearly constant: ≈ 3000 K [9]. Yet, the variation of T_e whose dynamic in pulsed plasma is a way faster than n_e [63] cannot be neglected. Supposing the possible increase of T_e from 0.2 eV to 1.0 eV (by extrapolating results in [63] for a given discharge conditions) and assuming Maxwell electron energy distribution, $\nu_{en}(t)$ increases approximately from 2E11 s^{-1} to 4E11 s^{-1}. It results in a falling trend of $1/\nu_{en}(t)$ which may contribute only to the reduction of P_{abs} and increase of P_{ref} (see Eq. 13). Therefore, the expected elevation of $\nu_{en}(t)$ due to increasing T_e in the beginning of pulse does not change qualitatively the discussed above dynamic of $P_{ref}(t)$: by hampering the absorption, the ν_{en} can only contribute to the amplitude of P_{ref} peak and its shift to a later time coordinate. Thus, among two fast responding factors, n_e and ν_{en}, the considered peaked behavior of reflected power in the beginning of pulse is supposed to be mostly driven by mean electron density evolution. At later times in the microwave pulse, P_{inc} is constant and a discharge enters a quasi-steady state, when $\langle T_e\rangle$ and $\langle n_e\rangle$ are also supposed to be constant. Some increase in the reflected power can be attributed to the possible change in n_e spatial distribution that may decrease the effective coupling volume and/or microwave matching quality – both lead to decrease of factor W_E in Eq. 13. Note, the time coordinates of that minimum: 33 ns, 74 ns and 1.39 us depend on t_{off} and correspond to t_{off} = 1.5 us, 6.0 us and 12.0 us, respectively (Fig. 11 b). The observed different timing of minimum position can be explained, by

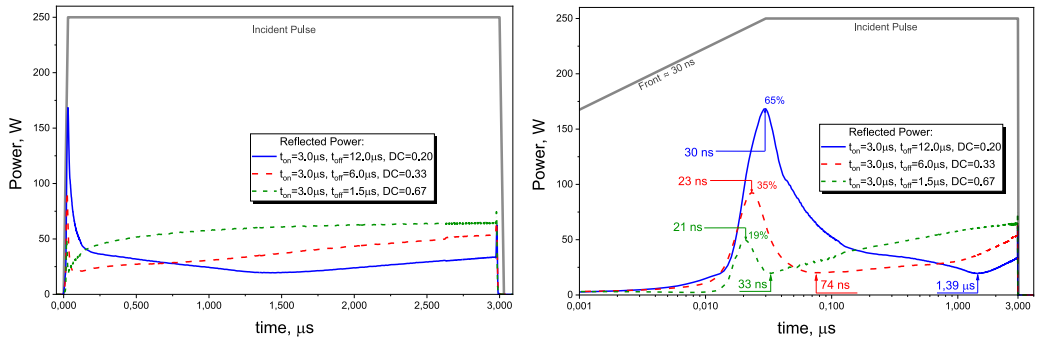


Fig. 11. Reflected power in coaxial torch experiment (plasma in reignition regime) with t_{on} = 2.0 μs and t_{off} = 12.0, 6.0 and 1.5 μs, or DC = 0.20, 0.33 and 0.67 respectively. Incident pulse is shown schematically with thick grey solid line. a) Linear scale. (b) Logarithmic scale to elucidate the evolution at the beginning of pulse. The times and amplitudes (percentage of incident power) for the first maximum are indicated as well as timing for minimum position.

the transient competition of still growing mean electron density $\langle n_e \rangle$ and microwave mismatch due to the change of n_e profile. Effectively, the position of this minimum in $P_{ref}(t)$ can be correlated with an ending time for n_e building-up phase. It is worth noting that at the end of pulse the reflected power jumps one more time (see Fig. 11 a), yet this increase is supposed to be related to the pulse propagation physics, which will be discussed in more detail in the next section.

3.3.2. *Time resolved reflected power in surfaguide-based reactor and plasma torch at IPP experiments*

In two kilowatt-range pulsed plasma experiments, Surfaguide-based reactor and the cavity-based plasma torch, the incident and reflected powers were measured using the same pulse power detectors as in coaxial-torch experiment. For energy decoupling from the main transmission line, a 50 dB bi-directional cross-guide coupler was utilized. The rising and falling edges of the incident power exhibit characteristic times of approximately 15 ns. Figs. 12 and 13 present the time traces for the incident and reflected power for operating conditions with t_{on}= 200 μs, t_{off}= 800 μs, P_{peak}= 4.3 kW and with t_{on}= 500 μs, t_{off}= 650 μs, P_{peak}= 4.07 kW, for the Surfaguide-based reactor and cavity-based plasma torch, respectively At the onset of the pulse, the reflected power exhibits a small perturbation, appearing as an overshoot in the cavity-based torch (Fig. 13b) and as an undershoot in the Surfaguide-based experiment (Fig. 12b), followed by steady-state levels of approximately 0.5% and 4.4% of the incident power, respectively. The overshoot amplitude in the cavity-based torch is relatively low, reaching about 1.2% of the incident power. In contrast, the initial peak observed in the coaxial plasma torch is significantly larger, ranging from approximately 20–65% of the incident power depending on the interpulse time t_{off} (see Fig. 11). In addition, a ringing feature at the beginning of the pulse is observed in both the incident and reflected power signals in the cavity-based torch. This behavior is likely associated with internal reflections within the waveguide structures, leading to interference effects. At the end of the microwave pulse, an overshoot is observed in the reflected power signals for both experimental configurations. The key difference compared to the reference coaxial torch is the absence of a pronounced spike at the beginning of the power-ON phase. In the coaxial case, the amplitude of this spike strongly depends on t_{off}, indicating a plasma re-ignition regime. In contrast, such behavior is not observed in the kilowatt-scale systems studied here. This suggests that a relatively high residual electron density persists during the power-OFF phase, enabling a smooth transition between power-OFF and power-ON states. This interpretation is further supported by the observation that the plasma remains well-developed throughout the entire modulation cycle (see Section 3.1.2). It is worth noting that a similar overshoot feature in the reflected power signal is also observed at the end of the pulse, exhibiting comparable amplitude and temporal width. Importantly, the amplitude of these spikes appears to be independent of the power-OFF time. This suggests that the observed perturbations are likely associated with wave propagation effects rather than intrinsic plasma dynamics. Components such as the 3-stub tuner, couplers, bends, and waveguide-to-coaxial adapters can induce the reflections and standing wave patterns if the impedances are not perfectly matched and the system attenuation is low.

To distinguish this from plasma effects on the reflected power, the microwave pulse propagation was simulated in a waveguide system with geometry relevant to real experiments. In Figs. 14 and 15, the simulated geometries for both plasma experiments consisting of H- and E-bends, 3-stub tuner, 50 dB bi-directional cross-guide coupler and plasma reactors are presented, respectively. The full-wave 3D simulations were performed with the aid of CST Studio Suite package from Dassault Systèmes [64]. The plasma column was simulated as the nested cylindrical objects each of which has the constant plasma permittivity ($\varepsilon_p' = 1 - \omega_p^2/(\omega^2 + \nu_{en}^2)$) and loss factor ($\varepsilon_p'' = \omega_p^2 \cdot \nu_{en}/(\omega^2 + \nu_{en}^2)$), where $\omega_p = 56.4\sqrt{n_e}$. The electron density profiles $n_e(r)$used in the model were manually constructed as stepwise functions for each experimental configuration, following a peaked radial distribution. The central electron density, 1×10^{19} m^{-3}, was based on interferometric measurements reported for similar conditions in [63], while the remainder of the profile was prescribed, with peripheral densities as low as 5×10^{15} m^{-3}. The constructed $n_e(r)$profiles for both experiments are shown in Fig. 16. The electron–neutral collision frequency was assumed to be constant over the radius, with a value of 1×10^{11} s^{-1}.The input port in both simulated geometries was excited with microwave pulse signal of 200 ns in length and frequency of 2.45 GHz. The corresponding response signals from forward (blue) and back propagating (orange) waves at two ports of bi-directional coupler are shown in Fig. 17. The simulated reflected power remains substantially below the incident power, amounting to approximately 0.4% of P_{inc} at the pulse flat-top, while about 99% of the incident power is absorbed within the plasma volume. The lower flat-top reflection predicted by the model (0.4%) compared with the experimental value (4.4%, Fig. 12) results from the optimized impedance matching of the three-stub tuner in the simulation. Nevertheless, the experimental reflection of approximately 4% still represents excellent power coupling between the microwave source and the plasma. The broadening of the reflected signal is evident and it is a known effect for pulse propagation in a waveguide [65]. Additionally, when the propagation path contains the elements, whose bandwidth is smaller than effective bandwidth of the incident microwave signal it initiates the reflections leading to the interference and, as a result, to amplitude perturbation in the beginning and in end of pulse. This modulation though needs to be distinguished from the observed much bigger relative variations in $P_{ref}(t)$ in the coaxial torch experiment, which originates from transient competition between load-mismatch reflection and electron density build-up after the breakdown. The observed pronounced transient P_{ref} peak in the beginning of pulse agrees with the results of Van Alphen et al. (see Fig. S13-S16 in [34]) and van

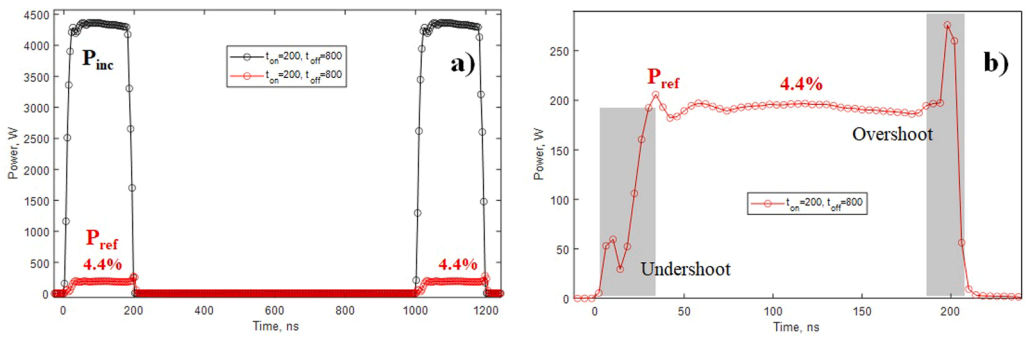


Fig. 12. Time traces for incident and reflected microwave power measured in Surfaguide-based reactor (no reignition) with t_{on} = 200 ns and t_{off} = 800 ns (DC=0.20) and peak power of 4.2 kW. (a) both $P_{inc}(t)$ *and* $P_{ref}(t)$ on a time span of 1300 ns, (b) $P_{ref}(t)$ on a time span of 220 ns. Mean level of P_{ref} in percentage of incident power is labeled.

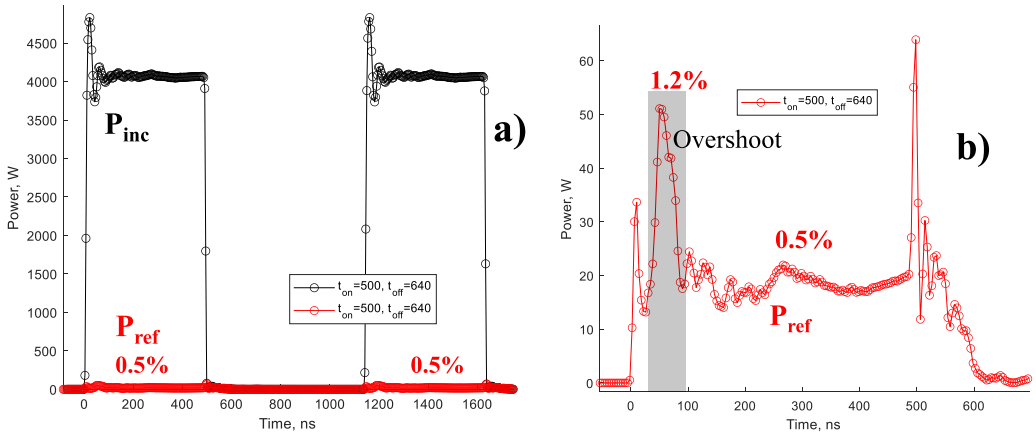


Fig. 13. Cavity-based plasma torch at IPP experiment with t_{on} = 500 ns and t_{off} = 640 ns (DC=0.437) and peak power of 4.07 kW and 7.5 slm CO2 inflow. (a) Time evolution of incident (black) and reflected (red) microwave power; (b) time trace of reflected power at time span of 700 ns. Mean level of P_{ref} in percentage of incident power is labeled.

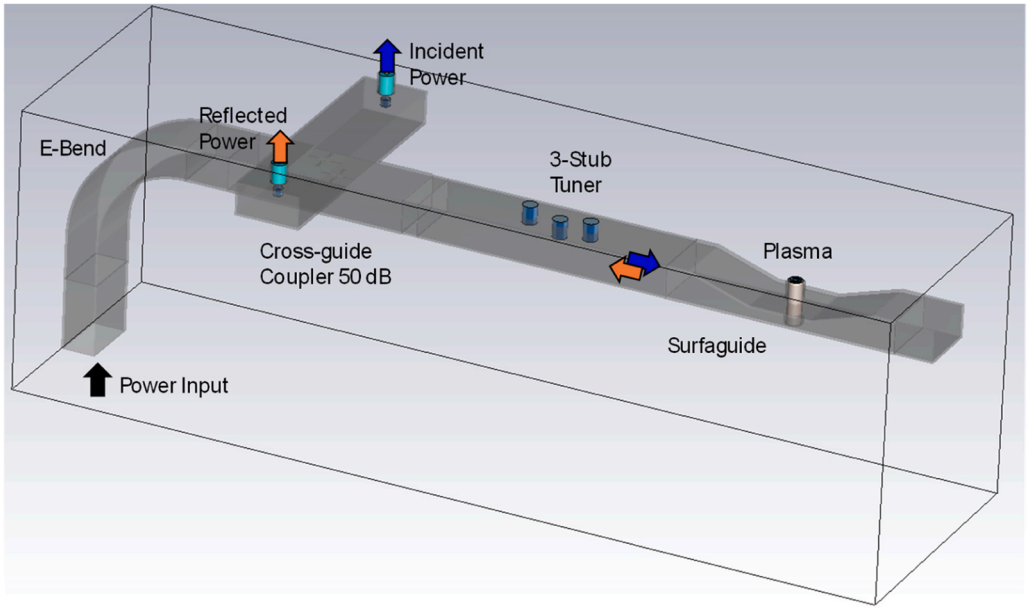


Fig. 14. Full-wave 3D model for microwave propagation within waveguide system of Surfaguide-based experiment including bends, 3-stub tuner, 50 dB bi-directional coupler and plasma reactor. Black and blue arrows indicate the forward propagation whereas orange arrow - back propagating wave.

de Steeg et al. [24], though obtained at vacuum conditions.

4. Summary and conclusions

Atmospheric-pressure CO_2 conversion under ultrafast microwave power pulsation was investigated in a Surfaguide-based reactor and a cavity-based plasma torch at IPP and compared with previous results from a compact coaxial torch. The two kW-scale reactors showed markedly different responses to power pulsation despite comparable peak microwave powers, highlighting the importance of reactor-specific plasma dynamics and post-plasma treatment. The main operating parameters and performance characteristics of the three systems are summarized in Table 4.

Because the three reactors operate over different *SEI* ranges, the effect of pulsation was assessed primarily relative to the corresponding CW operation within each reactor rather than by direct comparison at identical absolute power. The response to pulsation therefore reflects both SEI and reactor-specific plasma and post-discharge dynamics.

In the coaxial torch, pulsed operation produced a > 100% relative enhancement compared with CW operation. Time-resolved imaging and temperature measurements previously demonstrated repeated extinction/reignition, transient T_{vib}/T_{rot} nonequilibrium, and an increased effective plasma volume under pulsed excitation [9,26]. These observations indicate a less contracted pulsed discharge and distinguish this regime from those obtained in the two kW-scale reactors.

No comparable extinction/reignition regime was observed in either kW-scale reactor. In the Surfaguide-based reactor, plasma persistence during the power-OFF phase was confirmed by optical emission, while the reflected-power behavior of both kW-scale systems was consistent with a conducting plasma persisting between pulses. Stable operation was limited to $t_{off} \approx 12$ μs in the Surfaguide-based reactor and $t_{off} \approx 10$ μs in the cavity-based torch at IPP.

Note that the reignition regime was not attained in Surfaguide-based reactor. Within investigated duty cycle range ($0.25 < DC < 0.90$) plasma was continuously burning both in pulse and inter-pulse phases, that was confirmed with time resolved T_{vib}, T_{rot} and P_{ref} diagnostics. Although time-resolved temperature measurements were not available for the cavity-based torch at IPP, the time-resolved reflected-power signal

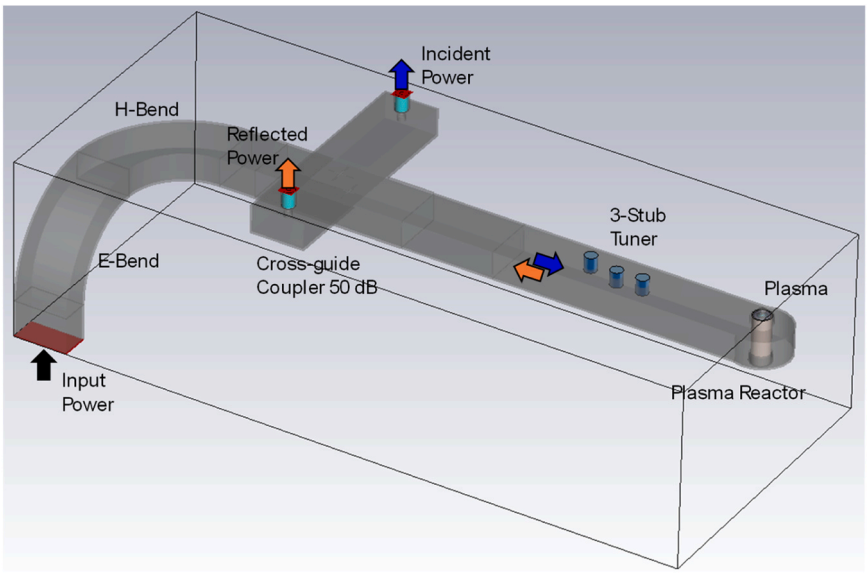


Fig. 15. Full-wave 3D model for microwave propagation within waveguide system in IPP Garching experiment including E- and H-bend, 3-stub tuner, 50 dB bi-directional coupler and plasma reactor with quartz tube and plasma inside. Black and blue arrows indicate the forward propagation whereas orange arrow back propagating wave.

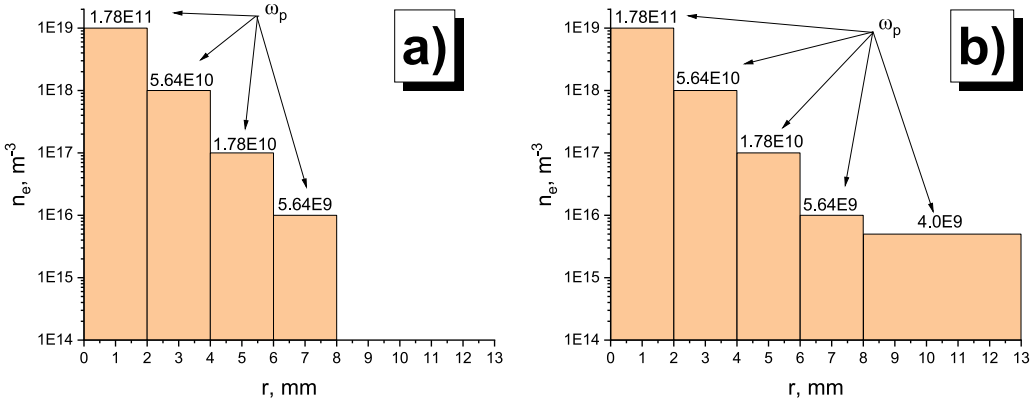


Fig. 16. Electron density profiles for simulated geometry of a) Surfaguide-based experiment (see Fig. 14) and b) plasma torch at IPP (see Fig. 15). Plasma frequency (ω_p) is labeled for corresponding radii and electron to neutral collision frequency is of 10^{11} s^{-1}.

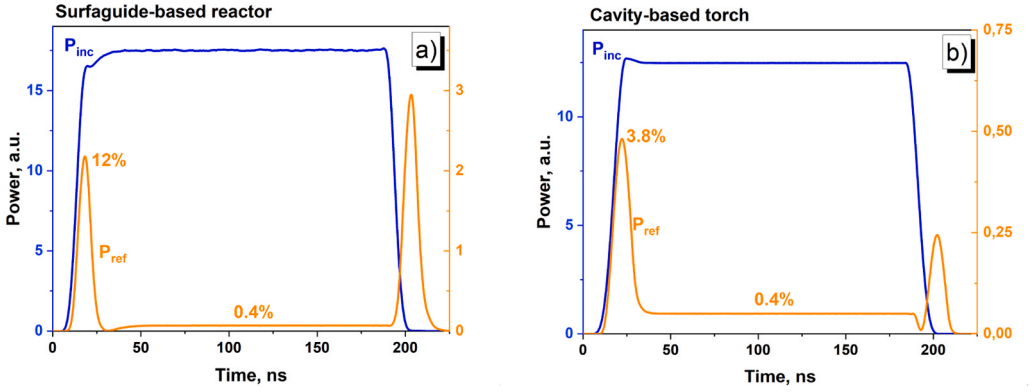


Fig. 17. Incident and reflected power at outputs of bidirectional coupler simulated for a) Surfaguide-based experiment (see Fig. 14) and b) plasma torch at IPP (see Fig. 15) geometries. Frequency is 2.45 GHz, t_{on} = 200 ns and rising and falling fronts are 15 ns.

provides independent evidence concerning plasma persistence between microwave pulses. Unlike the coaxial torch, where reignition is accompanied by a pronounced initial P_{ref} transient, no comparable reflection peak was observed in either of the 4-kW systems. For the Surfaguide-based reactor, the absence of extinction/reignition is additionally confirmed by the persistence of optical emission during the

Table 4
Comparison of setups, main parameters and performance of all three experiments considered.

	SEI, eV/ molec	E/n, Td	Peak power & plasma volume	Afterglow & Quenching	Pulse timing	Effects from microwave pulsation			
						n_e variation & Reignition	Plasma temperatures / nonequilibrium	Relative enhancement as compared with CW	Absolute χ, and η in pulsed mode
Coaxial torch	0.02 –0.22	65–75	220–260 W, V_{plas}= 0.05–0.15 cm^3	Gas expands in a bigger diameter tube	t_{on}= 0.5–50 μs DC= 0.10–0.99	Strong n_e variation due to reignition	T_{rot}= 3500–7500 K; T_{vib}= 6000–7500 K Nonequilibrium T_{vib}/T_{rot}≈ 2 [9]	Δχ~100%, Δη~130% ΔV_{plas}~50–100% [9]	~1%, η~27%
Surfaguide-based reactor (KIT)	0.7 – 2.7	10–40	3.0–4.2 kW V_{plas}< 30 cm^3 including expansion above the reactor	Slow moderate cooling in long quartz tube	t_{on}= 1.0–10 μs DC= 0.25–0.9	Seemingly small n_e variation based on $P_{ref}(t)$ No reignition	T_{rot}= 6000–7000 K T_{vib} = 7000–8500 K	Δχ~36% Δη~30% ΔT_{gas} ~13%	χ~15% η~25%
Cavity-based plasma torch (IPP)	1.5 – 5.0	10–40	4.05 kW V_{plas}≈ 23 cm^3	Fast, quick quenching in water-cooled nozzle	t_{on}= 0.5–10 μs DC= 0.22–0.62	Seemingly small n_e variation based on $P_{ref}(t)$ No reignition	T_{rot}= 5500–6000 K (only in CW)	No progress in χ, and η	χ~20% η~25% (same as in CW mode)

power-OFF phase. The similar limits of stable pulsed operation, $t_{off} \approx 12$ μs for the Surfaguide-based reactor and $t_{off} \approx 10.3$ μs for the IPP torch, further indicate that both kW-scale systems operate in a broadly similar plasma-persistence regime. This similarity does not, however, imply identical time-resolved gas-temperature evolution in the two reactors. At the same time, the progress in Surfaguide-based reactor performance shown in Fig. 8 looks quite promising and motivates further investigation of plasma regimes with longer t_{off} in future studies. Based on estimated T_{rot} cooling rate, inter-pulse times of several tens of μs would be required to achieve a temperature modulation depth equivalent to that observed in the coaxial torch experiment. However, such extended inter-pulse times imply operating the plasma in a reignition mode. Achieving this regime would likely necessitate a redesign of the current reactor configuration, the utilization of a more powerful microwave source, or both.

Microwave power pulsation may affect not only plasma chemistry but also radial transport and heat exchange within and downstream of the plasma region. Previous modelling studies [66–68] have shown that turbulent transport can enhance radial species and heat fluxes in contracted microwave plasmas. Although these processes were not directly measured in the present experiments, pulsing-induced modifications of gas-flow dynamics and radial transport could influence both the replenishment of the reactive plasma region and the post-plasma cooling of dissociation products.

In the Surfaguide-based reactor, no post-plasma quenching nozzle is present, and the hot plasma/afterglow extends downstream along the quartz tube, providing an extended region in which transport and post-plasma chemistry can influence the final gas composition. In contrast, the cavity-based torch at IPP is equipped with a water-cooled nozzle immediately downstream of the plasma region. Previous spatially resolved temperature measurements and validated fluid-dynamic/heat-transfer modelling for this reactor configuration [46] demonstrated that the nozzle strongly shortens the hot afterglow and rapidly reduces the gas temperature through enhanced mixing and heat transfer to the cooled nozzle walls. This difference may be particularly relevant to the response to microwave power pulsation. In the extended hot region of the Surfaguide-based reactor, pulsing-induced modifications of radial transport, turbulent mixing, heat transfer, and post-plasma chemistry have a comparatively large spatial region over which they may influence the final gas composition. In the cavity-based torch at IPP, the quenching nozzle strongly truncates this hot, chemically active region, thereby reducing the spatial and temporal opportunity for such pulsing-induced modifications to affect the outlet composition. This may contribute to the observation that pulsing enhances conversion and energy efficiency relative to CW operation in the Surfaguide-based reactor, whereas no corresponding enhancement is observed in the cavity-based torch at IPP.

The extent to which ultrafast microsecond-scale pulsing modifies radial transport, turbulent heat exchange, and post-plasma evolution cannot be quantified from the present measurements and remains a subject for future spatially resolved investigations.

The analysis of the reflected microwave power provides qualitative information on the evolution of the plasma electromagnetic load during power modulation. In the coaxial torch, plasma reignition produces a characteristic initial reflected-power peak associated with the developing plasma after power ON. In contrast, the absence of a comparable P_{ref} transient in the Surfaguide-based reactor and the cavity-based torch at IPP, together with the overall low reflected-power level, is consistent with the plasma remaining sufficiently conducting throughout the modulation cycle rather than returning to the extinguished state characteristic of the coaxial-torch reignition regime.

The microwave pulsation is believed to affect the electron component in atmospheric CO_2 plasma. Depending on reactor geometry, gas-flow pattern, microwave coupling, and afterglow configuration, microwave power pulsation may enhance thermal chemistry and transport processes or, as demonstrated previously for the coaxial torch, produce transient T_{vib}/T_{rot} nonequilibrium and reduced plasma contraction, which were associated with improved CO_2 conversion efficiency.

CRediT authorship contribution statement

S. Soldatov: Original Draft, Conceptualization, Methodology, Investigation, Formal Analysis, Software, Validation. **L. Silberer:** Writing - review & editing, Investigation, Validation. **C.K. Kiefer:** Writing - review & editing, Investigation, Validation, Formal analysis. **G. Link:** Writing - review & editing, Funding Acquisition, Resources, Project administration, Supervision. **A. Navarrete:** Writing - review & editing. **J. Jelonne:** Supervision, Funding Acquisition.

Declaration of Competing Interest

The authors declare that they have no known competing financial interests or personal relationships that could have appeared to influence the work reported in this paper.

Acknowledgements

The authors like to acknowledge Ante Hecimovic for organization and help in conduction of experiments at IPP site and for helpful discussions on the interpretation of observed physical effects. Vladislav Kotov is kindly acknowledged for insightful discussions on possible theoretical explanation of transient effects observed in pulsed plasma.

Data availability

Data will be made available on request.

References

[1] KEROGREEN (Production of sustainable aircraft grade kerosene from water and air powered by renewable electricity, through the splitting of CO_2, syngas formation and Fischer-Tropsch synthesis).2022; Available from: https://www.kerogreen.eu/.
[2] C.K. Kiefer, et al., CO2 dissociation using a lab-scale microwave plasma torch: An experimental study in view of industrial application, Chem. Eng. J. (2024) 481.
[3] R. Asisov, et al., Carbon Dioxide Dissociation in Non-Equilibrium Plasma. Proc. 5th Intern. Symp. Plasma Chemistry., 1981.
[4] Y.P.Z. Butylkin, V.K, E.G. Krasheninnikov, M.F. Krotov, V.D. Rusanov, Y. V. Tarasov, A.A. Fridman, Dissociation of CO2 by a plasma-chemical process in a nonequilibrium microwave discharge, Sov. Phys. - Tech. Phys. 26 (5) (1981).
[5] V.A. Legasov, et al., A nonequilibrium plasma-chemical process of CO_2 dissociation in high-frequency and ultrahigh-frequency discharges, Sov. Phys. Dokl. 23 (1978) 44.
[6] A. Berthelot, A. Bogaerts, Modeling of CO_2 Splitting in a Microwave Plasma: How to Improve the Conversion and Energy Efficiency, J. Phys. Chem. C. 121 (15) (2017) 8236–8251.
[7] F.A. D'Isa, et al., Performance analysis of a 2.45 GHz microwave plasma torch for CO_2 decomposition in gas swirl configuration, Plasma Sources Sci. Technol. 29 (10) (2020).
[8] G.J. van Rooij, et al., Taming microwave plasma to beat thermodynamics in CO2 dissociation, Faraday Discuss. 183 (2015) 233–248.
[9] S. Soldatov, et al., Time-Resolved Optical Emission Spectroscopy Reveals Nonequilibrium Conditions for CO_2 Splitting in Atmospheric Plasma Sustained with Ultrafast Microwave Pulsation, ACS Energy Lett. 6 (1) (2021) 124–130.
[10] E. Carbone, et al., Analysis of the C_2 ($d^3\Pi_g$-$a^3\Pi_u$) Swan bands as a thermometric probe in CO_2 microwave plasmas, Plasma Sources Sci. Technol. 29 (5) (2020) 055003.
[11] A. Fridman, Plasma chemistry, Cambridge university press, 2008.
[12] Abraham Jan Wolf, et al., Implications of thermo-chemical instability on the contracted modes in CO2 microwave plasmas, Plasma Sources Sci. Technol. 29 (2020) 11.
[13] N. den Harder, et al., Homogeneous CO2 conversion by microwave plasma: Wave propagation and diagnostics, Plasma Process. Polym. 14 (6) (2016).
[14] I. Belov, et al., Carbon dioxide dissociation in a microwave plasma reactor operating in a wide pressure range and different gas inlet configurations, J. CO2 Util. 24 (2018) 386–397.
[15] A. Hecimovic, et al., Enhancement of CO2 conversion in microwave plasmas using a nozzle in the effluent, J. CO2 Util. 57 (2022) 101870.
[16] A. Hecimovic, et al., Fast gas quenching of microwave plasma effluent for enhanced CO2 conversion, J. CO2 Util. 71 (2023).
[17] E.R. Mercer, et al., Post-plasma quenching to improve conversion and energy efficiency in a CO2 microwave plasma, Fuel 334 (2023).
[18] A. Rousseau, et al., Pulsed microwave discharge: a very efficient H atom source, J. Phys. D Appl. Phys. 27 (11) (1994) 2439.
[19] K. Hassouni, et al., Investigation of chemical kinetics and energy transfer in a pulsed microwave H2/CH4 plasma, Plasma Sources Sci. Technol. 10 (1) (2001) 61.
[20] E. Carbone, et al., Spatio-temporal dynamics of a pulsed microwave argon plasma: ignition and afterglow, Plasma Sources Sci. Technol. 24 (1) (2015) 015015.
[21] X. Duten, et al., Time-resolved measurements of the gas temperature in a H2/CH4 medium pressure microwave 915 MHz pulsed plasma, J. Phys. D Appl. Phys. 35 (16) (2002) 1939.
[22] V.A. Koldanov, et al., Self-consistent simulation of pulsed and continuous microwave discharges in hydrogen, Plasma Phys. Rep. 31 (11) (2005) 965–977.
[23] Y. Kabouzi, M. Moisan, Pulsed microwave discharges sustained at atmospheric pressure: study of the contraction and filamentation phenomena, IEEE Trans. Plasma Sci. 33 (2) (2005) 292–293.
[24] A.W. van de Steeg, et al., Plasma activation of N2, CH4 and CO2: an assessment of the vibrational non-equilibrium time window, Plasma Sources Sci. Technol. 29 (11) (2020) 115001.
[25] M. Baeva, et al., Pulsed microwave discharge at atmospheric pressure for NOx decomposition, Plasma Sources Sci. Technol. 11 (1) (2002) 1.
[26] S. Soldatov, et al., Efficiency of a compact CO2 coaxial plasma torch driven by ultrafast microwave power pulsing: Stability and plasma gas flow dynamics, J. CO2 Util. 58 (2022) 101916.
[27] M.S. Hernandez, et al., Overcoming thermal degradation during continuous conversion of water into hydrogen peroxide in a flexible plasma reactor, ChemRxiv (2026) 1–11.
[28] N. Britun, et al., Plasma-assisted CO2conversion: optimizing performance via microwave power modulation, J. Phys. D Appl. Phys. 51 (14) (2018) 144002.
[29] T. Silva, et al., Dynamics of Gas Heating in the Afterglow of Pulsed CO2 and CO2–N2 Glow Discharges at Low Pressure, Plasma Chem. Plasma Process. 40 (3) (2020) 713–725.
[30] S. Hübner, et al., A power pulsed low-pressure argon microwave plasma investigated by Thomson scattering: evidence for molecular assisted recombination, J. Phys. D Appl. Phys. 45 (5) (2012) 055203.
[31] M.A. Lieberman, S. Ashida, Global models of pulse-power-modulated high-density, low-pressure discharges, Plasma Sources Sci. Technol. 5 (2) (1996) 145.
[32] D.C.M. van den Bekerom, et al., The importance of thermal dissociation in CO2 microwave discharges investigated by power pulsing and rotational Raman scattering, Plasma Sources Sci. Technol. 28 (5) (2019) 055015.
[33] V. Vermeiren, A. Bogaerts, Improving the Energy Efficiency of CO2 Conversion in Nonequilibrium Plasmas through Pulsing, J. Phys. Chem. C. 123 (29) (2019) 17650–17665.
[34] S. Van Alphen, et al., Power Pulsing To Maximize Vibrational Excitation Efficiency in N2 Microwave Plasma: A Combined Experimental and Computational Study, J. Phys. Chem. C. 124 (3) (2019) 1765–1779.
[35] M. Moisan, Z. Zakrzewski, Plasma sources based on the propagation of electromagnetic surface waves, J. Phys. D Appl. Phys. 24 (7) (1991) 1025–1048.
[36] K. Wiegers, et al., Determination of the Conversion and Efficiency for CO in an Atmospheric Pressure Microwave Plasma Torch, Chem. Ing. Tech. 94 (3) (2022) 299–308.
[37] M. Leins, et al., Studies on a Microwave-Heated Atmospheric Plasma Torch, Plasma Process. Polym. 4 (2007) S493–S497.
[38] TRUMPF. *TRUMPF Microwave Generators*. 2026 [cited 2026; Microwave Generators]. Available from: https://www.trumpf.com/de_DE/produkte/leistungselektronik/generatoren-zur-industriellen-erwaermung/truplasma-mw-serie-1000-3000-5000/.
[39] Heuermann, Plasma jets of the PS-series (cited), Heuermann HF-Technik GmbH, 2026 (Available from: https://hhft.de/jets-ps-serie).
[40] F. D'Isa, et al., Performance analysis of a 2.45 GHz microwave plasma torch for CO2 decomposition in gas swirl configuration, Plasma Sources Sci. Technol. (2020).
[41] R. Antunes, et al., Proof of Concept for O Removal with Multiple LCCF Membranes Accommodated in the Effluent of a CO Plasma Torch, Acs Sustain. Chem. Eng. 11 (44) (2023) 15984–15993.
[42] A. Schulz, et al., Scalable Microwave Plasma Sources From Low to Atmospheric Pressure, Contrib. Plasma Phys. 52 (7) (2012) 607–614.
[43] M. Leins, et al., Microwave Plasmas at Atmospheric Pressure, Contrib. Plasma Phys. 54 (1) (2014) 14–26.
[44] A. Hecimovic, et al., Quantitative gas composition analysis method for a wide pressure range up to atmospheric pressure-CO plasma case study, Rev. Sci. Instrum. 91 (11) (2020).
[45] A. Hecimovic, et al., Enhancement of CO conversion in microwave plasmas using a nozzle in the effluent, J. Co2 Util. 57 (2022).
[46] S. Van Alphen, et al., Modelling post-plasma quenching nozzles for improving the performance of CO2 microwave plasmas, Chem. Eng. J. 462 (2023).
[47] J. Voráč, et al., Batch processing of overlapping molecular spectra as a tool for spatio-temporal diagnostics of power modulated microwave plasma jet, Plasma Sources Sci. Technol. 26 (2) (2017) 025010.
[48] J. Vorác, et al., State-by-state emission spectra fitting for non-equilibrium plasmas: OH spectra of surface barrier discharge at argon/water interface, J. Phys. D. -Appl. Phys. 50 (29) (2017).
[49] A. Böhle, et al., Pulsed discharges produced by high-power surface waves, J. Phys. D Appl. Phys. 29 (2) (1996) 369.
[50] Boonton Electronics Oct 2021]; Available from: https://www.boonton.com/products/rf-power-sensors/rtp5000-real-time-peak-power-sensors.
[51] Emerson Manual X-STREAM XEGP gas analyser 2013.
[52] B. Wanten, et al., Plasma-based CO2 conversion: How to correctly analyze the performance? J. Energy Chem. 86 (2023) 180–196.
[53] C.K. Kiefer, Efficiency of microwave plasmas for conversion of greenhouse gases (CO2, CH4) towards value-added chemicals, Universität Augsburg University, PhD,2025.
[54] V. Kotov, Vibrational relaxation and triggering of the non-equilibrium vibrational decomposition of CO2 in gas discharges, Plasma Sources Sci. Technol. 31 (9) (2022) 094002.
[55] J.S. Bendat, A.G. Piersol, Random Data: Analysis And Measurement Procedures, 640, John Wiley & Sons, 2011.
[56] I.H. Hutchinson, Principles of Plasma Diagnostics, Cambridge University Press, 2002.
[57] V. Vermeiren, A. Bogaerts, Plasma-Based CO2 Conversion: To Quench or Not to Quench? J. Phys. Chem. C. 124 (34) (2020) 18401–18415.
[58] V.Va.A. Bogaerts, Plasma-Based CO2 Conversion: To Quench or Not to Quench? J. Phys. Chem. C. 124 (34) (2020) 18401–18415.
[59] M.A. Heald, C.B. Wharton, Plasma diagnostics with microwaves, Wiley & Sons, New York, 1965.
[60] Y.P. Raizer, Gas discharge physics, Springer, Berlin, 1991.
[61] L. Silberer, Electron density estimation in atmospheric microwave plasma by means of transmitted signal phase measurements with V-band vector network analyzer. Institute for Pulsed Power and Microwave Technology, Karlsruhe Institute of Technology (KIT), 2022, p. 75.
[62] P.W.C. Groen, et al., Numerical model for the determination of the reduced electric field in a CO2 microwave plasma derived by the principle of impedance matching, Plasma Sources Sci. Technol. 28 (7) (2019) 075016.

[63] E. Carbone, S. Nijdam, Ultra-fast pulsed microwave plasma breakdown: evidence of various ignition modes, Plasma Sources Sci. Technol. 23 (1) (2014) 012001.
[64] *Dassault Systèmes, CST Studio Suite*. 27.02.2026]; Available from: https://www.3ds.com/products/simulia/cst-studio-suite.
[65] R.D. Wanselow, Rectangular pulse distortion due to a nonlinear complex transmission propagation constant, J. Frankl. Inst. 274 (3) (1962) 178–184.
[66] V. Kotov, C. Kiefer, A. Hecimovic, Validation of the thermo-chemical approach to modelling of CO2 conversion in sub-atmospheric pressure microwave gas discharges, Plasma Sources Sci. Technol. 33 (6) (2024) 065012.
[67] H.M.S. Van Poyer, et al., Influence of radial transport and turbulent effects on CO2 conversion in a microwave plasma reactor: insights from a multi-dimensional thermo-chemical flow model, Chem. Eng. J. 507 (2025) 160688.
[68] V. Laitl, et al., Fluid–electromagnetic modelling of atmospheric pressure CO2 microwave plasma: towards reactor design, Chem. Eng. J. 526 (2025) 171039.